PV Reference Cells for Outdoor Use: Comparison of First-Year Field Measurements

Anton Driesse

PV Performance Labs

NREL Technical Monitors: Peter Gotseff and Manajit Sengupta

NREL is a national laboratory of the U.S. Department of Energy
Office of Energy Efficiency & Renewable Energy
Operated by the Alliance for Sustainable Energy, LLC

This report is available at no cost from the National Renewable Energy Laboratory (NREL) at www.nrel.gov/publications.

Contract No. DE-AC36-08GO28308

Subcontract Report
NREL/SR-5D00-82086
May 2022

PV Reference Cells for Outdoor Use: Comparison of First-Year Field Measurements

Anton Driesse

PV Performance Labs

NREL Technical Monitors: Peter Gotseff and Manajit Sengupta

Suggested Citation
Driesse, Anton. 2022. *PV Reference Cells for Outdoor Use: Comparison of First-Year Field Measurements*. Golden, CO: National Renewable Energy Laboratory. NREL/SR-5D00-82086. https://www.nrel.gov/docs/fy22osti/82086.pdf.

NREL is a national laboratory of the U.S. Department of Energy
Office of Energy Efficiency & Renewable Energy
Operated by the Alliance for Sustainable Energy, LLC

This report is available at no cost from the National Renewable Energy Laboratory (NREL) at www.nrel.gov/publications.

Contract No. DE-AC36-08GO28308

Subcontract Report
NREL/SR-5D00-82086
May 2022

National Renewable Energy Laboratory
15013 Denver West Parkway
Golden, CO 80401
303-275-3000 • www.nrel.gov

NOTICE

This work was authored in part by the National Renewable Energy Laboratory, operated by Alliance for Sustainable Energy, LLC, for the U.S. Department of Energy (DOE) under Contract No. DE-AC36-08GO28308. Funding provided by U.S. Department of Energy Office of Energy Efficiency and Renewable Energy Solar Energy Technologies Office. The views expressed herein do not necessarily represent the views of the DOE or the U.S. Government.

Acknowledgments

This work was authored by Anton Driesse of PV Performance Labs Germany for the Alliance for Sustainable Energy, LLC, the manager and operator of the National Renewable Energy Laboratory for the U.S. Department of Energy under Contract No. DE-AC36-08GO28308.

The author gratefully acknowledges the contributions of the National Renewable Energy Laboratory's Solar Radiation Research Laboratory staff Pete Gotseff and Afshin Andreas, who spent countless hours acquiring, mounting, wiring, configuring, and ensuring the correct operation of the many test devices and calibrating and maintaining all the reference instruments needed for the evaluations; as well as Manajit Sengupta and Aron Habte for providing funding, organization, and many strategic discussions. Constructive comments and suggestions from reviewers Michael Gostein, Justin Robinson, Frank Vignola, and Stefan Wilbert are also very much appreciated.

List of Acronyms

AOI	angle of incidence
BORCAL	Broadband Outdoor Radiometer Calibration
IEC	International Electrotechnical Commission
Modbus	Modicon communications protocol
NREL	National Renewable Energy Laboratory
PV	photovoltaic
SRRL	Solar Radiation Research Laboratory
WPVS	World Photovoltaic Scale

Executive Summary

Reference cells are widely used in the photovoltaic (PV) industry to measure irradiance. For field applications and outdoor use a variety of products are on the market and they are often perceived as low-cost alternatives to thermopile pyranometers. But reference cell characteristics, such as directional and spectral response, fundamentally differ from pyranometers; therefore, measurements made by the former cannot be substituted for or directly compared with the latter. The National Renewable Energy Laboratory's (NREL's) Solar Radiation Research Laboratory is currently in a multiyear effort to develop guidance and recommendations for the design and use of outdoor reference cells, with a view to reducing inconsistencies and measurement uncertainty. The core of this effort is the long-term deployment of multiple products from different manufacturers, which are mounted at a fixed tilt, on a single-axis tracker, and on a dual-axis tracker.

This report provides an analysis of the data collected during the first year of operation at the NREL location. An overall assessment is made by comparing the total energy measured by each instrument to the other instruments having the same orientation. These totals are calculated for three different scenarios: (1) using the factory calibration factors, (2) using the previously determined NREL Cell Lab calibration factors, and (3) using the newly determined field calibration factors derived from the recorded measurements. Because the true or correct measurement values are unknown, pair-wise comparisons are made. The results show that the difference between the highest and lowest measured energy can exceed 3% when using the factory calibration factors. Consistency among instruments improves when Cell Lab calibrations are used, and it further improves when using field calibration factors.

To compare individual 1-minute measurements, a reference signal is constructed using a weighted average of multiple sensors. Deviations from the reference are then plotted both on sun path diagrams and time-series charts, which makes it possible to identify specific causes and consequences of systematic deviations, such as directional response, nonlinearity, spectral response, and temperature response. Although the median 1-minute deviations are similar to the differences observed in the annual energy, the *range* of 1-minute deviations varies substantially among products. For some products in tracking configurations, 95% of the deviations are well within 1% of the reference signal, suggesting the level of consistency that is achievable. But more typically this 95% inter-quantile range extends from 2%–3% positive to 3%–4% negative deviations.

One product with built-in electronics was evaluated and found to exhibit substantial offset error. Digital devices such as this are frequently used in industry because they are easy to integrate into systems, but they are more complex and have additional sources of potential measurement error; thus, the scope of this project should be extended to include the evaluation of digital devices.

PV reference cells lack a clear and complete specification of their measurand—the quantity they measure. Such a specification is needed to give manufacturers of reference devices clear objectives to pursue and to give users clear criteria to evaluate, compare, and choose products. In addition, a defined behavior will permit the role of diffuse irradiance in calibration to be clarified.

Table of Contents

List of Figures

List of Tables

1 Introduction

During 2019, the National Renewable Energy Laboratory's (NREL) Solar Radiation Research Laboratory (SRRL) acquired 39 commercial reference cell products of varying designs from different manufacturers. Upon receipt, they were first exposed outdoors for a period of preconditioning, and subsequently calibrated and characterized at the NREL Cell Lab. Many were also evaluated during one or more of the 2019 Broadband Outdoor Radiometer Calibration (BORCAL) sessions (Driesse 2021). Most cells were subsequently installed outdoors for continuous monitoring at SRRL, and a smaller set was sent to the University of Oregon for monitoring there (Vignola et al. 2021).

This report examines the measurements collected during the first full year of operation at SRRL. The focus is on identifying and understanding differences among products that affect the measurements. These differences are examined first in the form of annual summaries and subsequently as quantities that vary with time and sun position. This report is a catalogue of observations from which the authors derive certain observations and conclusions but which also provides ample opportunity for readers to develop their own.

From a user's point of view, differences among products are usually undesirable because all products exist to measure the same quantity. In principle, reference cells should be similar to the photovoltaic (PV) modules with which they are used, but in practice the information needed to quantify such similarity is unavailable. A useful and achievable alternative is to have reference cells that are similar to each other. Differences among products have been identified and characterized in previous projects, such as Driesse and Zaaiman (2015), and they also became quite apparent during the 2019 BORCAL calibrations. A comprehensive report on calibrations and a discussion of reference cell characteristics is found in Driesse (2021).

A fundamental challenge in the comparison and evaluation of reference cells is the lack of precise, formal specification of the measurand—the quantity that is being measured—in outdoor applications. Without such a specification, it is difficult to evaluate measurement error or measurement uncertainty in outdoor operation. The usual name given to the measurand is *effective irradiance*, which is a quantity proportional to the light-generated current in the cell, and for practical purposes, it is equal to the short-circuit current (I_{sc}) of the cell. This is the operating principle of all these products: They measure the short-circuit current of a small PV cell; thus, effective irradiance is a label rather than a definition of the measurand. To circumvent this lack of definition, this report makes relative comparisons among the products.

2 Sensors and Equipment

The PV reference cells at SRRL are divided into three groups, which are mounted at different orientations: 40° fixed-tilt facing south (S40), single-axis tracking (TR1), and dual-axis tracking (TR2). Each orientation also includes a broadband pyranometer and a pair of photodiodes, and the trackers each have a pair of spectroradiometers, which are shown in Figure 1.

Figure 1. Reference cells installed for field observations at the SRRL. *Photos by NREL*

One set is tilted at 40° south (left), and one set is on a dual-axis tracker (right). The third set is on a single-axis tracker (not shown, but it is similar to the dual-axis tracker).

This report focuses on the monocrystalline and two polycrystalline cells—eight types from six manufacturers, as identified in Table 1.

Table 1. Sensor Types Evaluated

Company	Model	Subtype	Short ID	Fixed Tilt	Single Axis	Dual Axis
Atonometrics	810226-02	Mono	RC18	Yes	Yes	Yes
EETS	RC01	Mono	RC01	Yes	Yes	Yes
Fraunhofer ISE	511311102	Mono	WPVS	Yes		Yes
IKS Photovoltaik	ISET	Mono	ISET	Yes	Yes	Yes
IKS Photovoltaik	ISET-poly	Poly	ISET-P	Yes		
IMT	Si-mV-85-PT1000	Mono	Si2	Yes	Yes	Yes
NES	SOZ-03	Mono	SOZ-03	Yes	Yes	Yes
NES	SOZ-03-P	Poly	SOZ-03-P	Yes		

2.1 Analog Versus Digital Outputs

Our objective in this work is to study the signals produced by reference cells in their most basic form—that is, the raw voltage or current signals without processing by amplifiers or other electronics. The scientific reason to work with the raw signals is to be able to identify strengths, weaknesses, and differences related to the core materials and physical designs of the products. Amplifiers or other

electronics can have their own unique characteristics that could mask or modify these differences. Of course, we understand that many reference cell products deployed by industry in recent years contain electronics and offer a digital interface; therefore, we aim to follow up the present work with separate evaluations of these aspects as well.

One manufacturer (Atonometrics) does not offer a version of its product (RC18) without electronics; therefore, the signals we evaluate for this report are not the raw analog signals from its PV cell. Internally, the RC18 measures the voltage across a shunt resistor, just like we do externally for all the other sensors. The RC18 then converts this voltage from analog to digital form and makes the digital value of the short-circuit current (I_{sc}) available via Modbus. It also reconverts the digital value to an analog output voltage for use with analog data loggers; thus, the analog signals used in our evaluation have been converted twice.

The factory specifications pertaining to the conversion electronics are: nonlinearity ±0.03% of range, repeatability ±0.02% of range, calibration ±0.1% of reading, and ±0.2% of range. The last item is the dominating factor equating an uncertainty of 3 mV on the 1.5-V output scale, which represents approximately 3 W/m^2. Some portion of this uncertainty arises in the analog-to-digital conversion stage, thus affecting both analog and digital outputs equally; and the remainder is attributable to the analog output stage, affecting only the analog output; thus, the analog output carries a higher uncertainty than the digital output. However, this higher uncertainty value is still low in the context of typical overall irradiance measurement uncertainties; therefore, we elected to capture the analog signals for both I_{sc} and temperature from each RC18 in the same way we captured the analog signals from the other products. It is clear, however, that all observations about the RC18 in this report are about the whole product, including the electronics.

Finally, the RC18 offers the option to obtain temperature-corrected W/m^2 as analog output. We chose to collect I_{sc} instead and apply the calibration factor and manufacturer-recommended temperature correction in a subsequent calculation. This is a standard mathematical step and produces the same result whether done within the RC18 or within the data logger.

2.2 Data Collection, Quality Control, and Filtering

All sensors are connected to the Measurement and Instrumentation Data Center infrastructure at the SRRL (Stoffel and Andreas 1981). The irradiance signal, V, and temperature, T, of each sensor are measured every 2 or 3 seconds, and the temperature-corrected irradiance, G_{eff}, is calculated using the manufacturers' calibration factor, R, and the temperature coefficient, α, using the following equation:

$$G_{eff} = \frac{V}{R \cdot (1 + \alpha \cdot (T_{cell} - 25)} \quad (1)$$

For all three signals, the 1-minute averages as well as the top-of-the-minute values are collected and stored. The latter are closely synchronized with the 1-minute readings from the spectroradiometers for the evaluation of spectral mismatch.

All sensors are cleaned once on most regular working days of the year; thus, accumulation of soiling is minimal. On some occasions, however, substantial amounts of snow caused differences in the irradiance reported by different sensors.

To explore the systematic differences among sensors, occasional large and unexplained differences can and should be ignored. These can occur as the result of cleaning and maintenance or through the influence of birds, insects, and other wayward creatures. For each group of sensors (fixed tilt, single-axis tracking, and dual-axis tracking), the envelope for acceptable values is set at the median value of the group ±(5% + 20 W/m^2). If one sensor is outside this range, all measurements at this time stamp are masked. Nighttime readings and time stamps that have any values less than 5 W/m^2 are also masked. These thresholds were set based on manual inspection of the data. The proportion of accepted data is approximately 94% of daytime values for the sensors mounted on the trackers and 88% for those at fixed tilt. These are high proportions; therefore, the accepted data can be considered representative of the full range of conditions in 1 year.

During quality control, it became apparent that the I_{sc} signals from the RC18 units do not go down to zero at night when there is no solar irradiance but remain at 2–3 mV. Our investigation found two reasons for this: First, the ground potential at the RC18 is higher than at the logger because of a voltage drop in the RC18 cable. Second, the RC18 produces a non-zero analog output signal at night. The first offset can and should be avoided by using a differential measurement rather than a single-ended measurement on the data logger, but the second offset is inherent to the RC18 analog output.

The voltage drop in the cable that causes the offset for the single-ended measurement can be calculated and subtracted from the logger signal. The copper leads have a resistance, R_o, of approximately 0.8 Ω and a temperature coefficient α = 0.4%/°C; the RC18 current draw, I_{RC18}, is reasonably stable near 4.8 mA, and the ground current is divided over two leads (signal and power ground); therefore, the voltage error is:

$$v_{err} = \frac{I_{RC18} \cdot R_0}{2} \cdot (1 + \alpha \cdot T_{amb}) \quad (2)$$

At 0°C, this calculated error is 1.92 mV, representing approximately 2 W/m^2. For this report, the analog signals collected from the three RC18 units are corrected by subtracting these calculated error values. After the correction, the nighttime signals range from 0.4–1.4 mV, which appears to be the inherent RC18 minimum voltage output. This is comparable to two RC18 units deployed at the University of Oregon that are measured differentially and produce nighttime analog values of approximately 1.35 mV.

On 2022-01-18, all RC18s deployed at SRRL were connected by Modbus so that the corrected analog signals could be compared to the digital readings. Using 10 days of daytime data, a linear regression of digital against analog readings was performed to quantify the difference. Results are presented in Table 2. The offset on the unit mounted at fixed tilt is near the limit of the specified uncertainty, but overall the differences are small.

Table 2. Results of Linear Regression, RC18 Digital Against Analog Values >5 mV (digital = analog * gain + offset)

Orientation	Gain (-)	Offset (mV)	RMSE[a] (mV)
Two-axis tracker (TR2)	0.9986	0.10	1.38
One-axis tracker (TR1)	0.9998	2.36	0.82
Fixed tilt (S40)	0.9996	3.04	0.51

[a] Root mean square error

2.3 Field Calibration

Although no explicit calibration procedure was carried out during the year,[1] there were many days with good, clear calibration conditions; thus, a virtual field calibration can be done for each group by simply comparing their readings during these suitable intervals. For sensor intercomparison, an absolute calibration is not really needed; therefore, at each suitable time stamp, the mean value of the readings in each group is used as the reference irradiance. The output of this virtual calibration is a scaling factor for each sensor that can be used to post-adjust all its irradiance values and thereby simulate an alternate calibration.

The criteria for selecting suitable data points are guided by the requirements in International Electrotechnical Commission 60904-2 (IEC 2015) and ASTM E1362 (ASTM 2015), which are listed in Table 3. Most conditions are met or exceeded. ASTM is somewhat more difficult to satisfy because it requires temperature control, which is not usually done for field deployment. ASTM also requires dual-axis tracking, but with the large amount of data available, it is possible to choose points with the sun nearly normal to the cells for the single-axis and fixed-tilt orientations, thereby achieving the same objective.

The absence of clouds is not verified to the extent required by the standard. It would be possible to go back and check this using the available sky camera records, but the accepted data points show such good consistency that this is deemed unnecessary for the present purpose. The only step taken to avoid egregious cloud enhancement effects is to require 5 minutes of stable conditions before and after the accepted data points. Finally, weekend data were rejected because the sensors were only cleaned on regular working days.

Altogether, the constraints discussed here and listed in Table 3 yield approximately 200 and 400 sets of valid readings spanning periods from 4–6 weeks for the fixed-tilt and tracking systems, respectively. The ratios of these readings were averaged to produce relative calibration factors of very good consistency, with standard deviation <0.1% for every sensor.

[1] A carefully planned procedure for the spring equinox was thwarted by snowfall.

Table 3. Outdoor Calibration Conditions

IEC 60904-2 Ed.3	ASTM E1362-15	This Work
Clear, sunny, and diffuse fraction <20%	Clear	Diffuse fraction <20%
No observable cloud formations	No observable cloud formations within a 30° half-angle cone surrounding the sun	5 minutes of stable conditions required before and after valid readings (dG/dt <1% per minute)
	Use a collimator *or* avoid excessive reflections from ground and nearby objects.	Foreground albedo is low; no foreground obstacles
Total irradiance ≥800 W/m^2	Total irradiance >750 W/m^2 and <1100 W/m^2	Total irradiance >800 W/m^2 and <1100 W/m²
Air mass between AM1 and AM2		Air mass between AM1.2 and AM1.5
Angle of incidence ≤5.0°	Angle of incidence <0.5° (tracking)	Angle of incidence ≤5.0°
Coplanar ±1.0°	Coplanar	Coplanar ±0.5°
Temperature correction to 25°C	Temperature controlled at 25°C ±2°C	Temperature correction to 25°C
Spectral mismatch correction as needed	Spectral mismatch correction (no more than 20% adjustment)	Spectral correction using measured global normal spectra
Five sets of readings, twice per day on 3 separate days	Three sets of readings	200–500 sets of readings spread throughout 4–6 weeks
Less than 0.5% variation in signal ratio over five sets	Standard deviation of signal ratios ≤1.0%	Standard deviation of signal ratios <0.1% *(achieved value)*

Note: The calibration of a reference cell is normally linked to the World Radiometric Reference through collimated, normally incident radiation only. When an outdoor secondary calibration is carried out, some diffuse light is permitted by the standards—presumably because it would not greatly affect the results. Indeed, if the directional responses of the two devices is the same, this should not affect the result of the calibration; however, if the directional responses of the calibration reference and the device under test differ, then an outdoor calibration including diffuse light can produce a slightly different calibration factor from a calibration procedure using only collimated light. The reference cells in this study do not have identical directional responses; therefore, some systematic differences can be expected.

3 Comparisons of Annual Energy

The first comparison of the reference cells is based on integrated effective irradiance (effective energy) in the plane of array measured during the 1-year period from May 2020 to April 2021. These totals will naturally be different for the three orientations; therefore, the direct comparison is only possible within each group, but five sensor types are repeated in all three groups for broader observations.

The true total of the effective energy for each orientation is unknown, but it likely lies somewhere between the observed extremes. To avoid making assumptions about the true values, the differences between sensors are calculated pair-wise in each group and scaled as a percentage of the overall mean. These percentage differences are placed on a grid to allow for comparisons between any pair. Taking Figure 2 as an example, the second column shows how the RC01 measured 0.48% more energy than the ISET in row one but 0.04% less than the WPVS in row six. The percentage difference from the overall mean for each sensor is also calculated and shown in the bottom row.

Of course, the measured energy is directly proportional to the calibration factor used for each cell, so it is easy to scale the annual totals and thereby create different calibration scenarios. The result on the percentage differences, however, is not a simple scaling but more like a redistribution. Three scenarios are shown in the following sections: (1) using the original factory calibrations, (2) using the NREL Cell Lab calibrations, and, (3) using the new field calibration factors. Figure 2 through Figure 10 show the results of the three calibration scenarios for the three sensor orientations and are followed by observations and discussion.

3.1 Dual-Axis Tracker

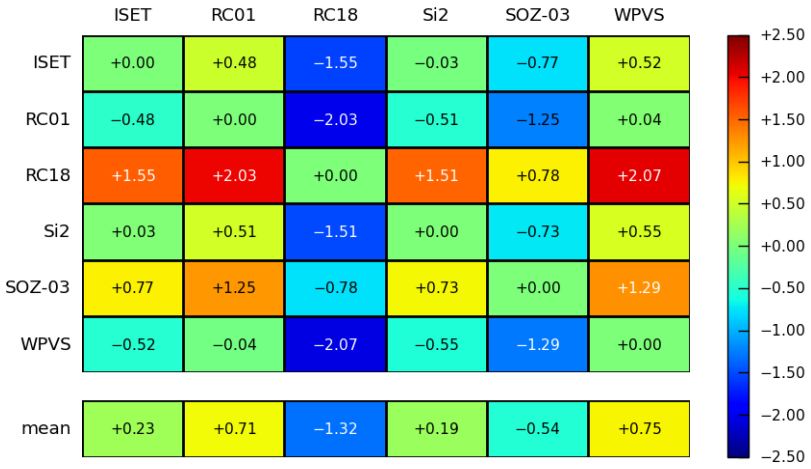

Figure 2. Differences in total energy measured on the dual-axis tracker using *factory* calibration factors

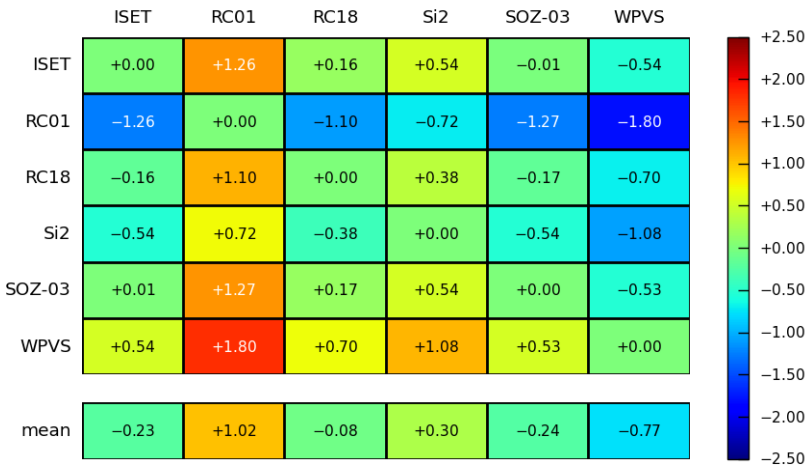

Figure 3. Differences in total energy measured on the dual-axis tracker using *NREL Cell Lab* calibration factors

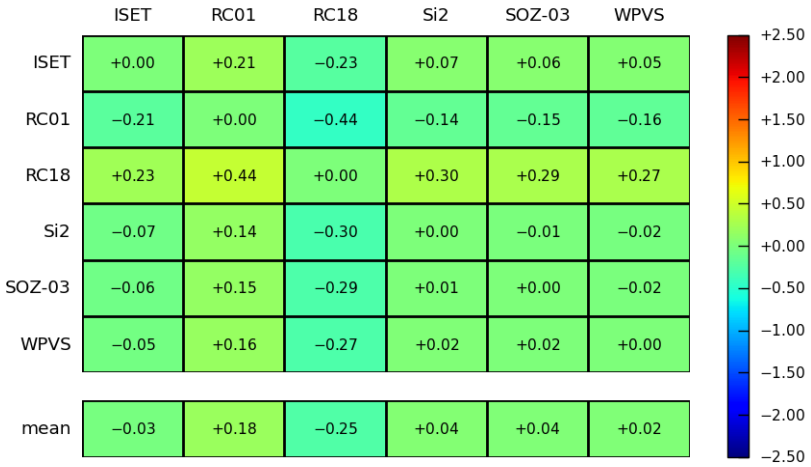

Figure 4. Differences in total energy measured on the dual-axis tracker using *field* calibration factors

3.2 Single-Axis Tracker

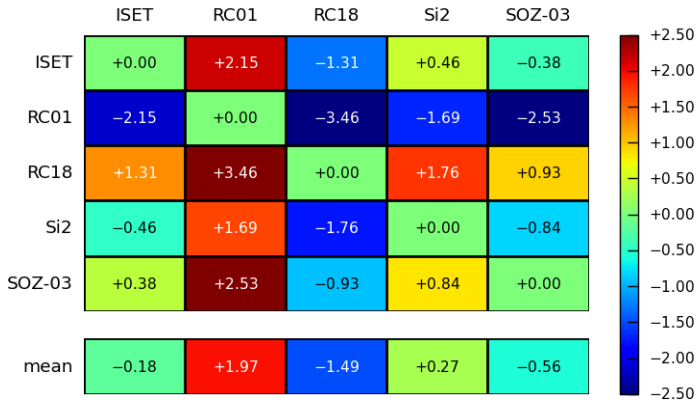

Figure 5. Differences in total energy measured on the single-axis tracker using *factory* calibration factors

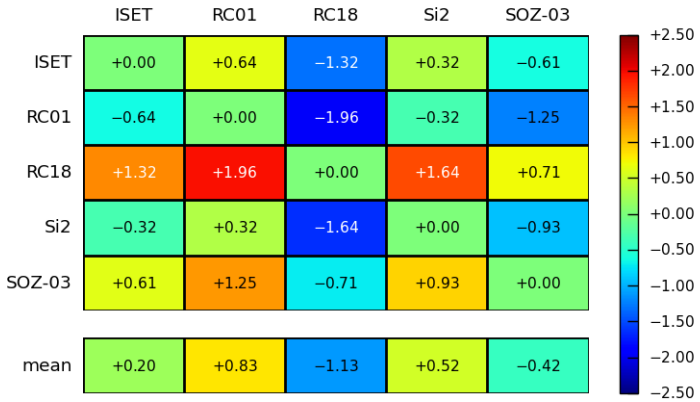

Figure 6. Differences in total energy measured on the single-axis tracker using *NREL Cell Lab* calibration factors

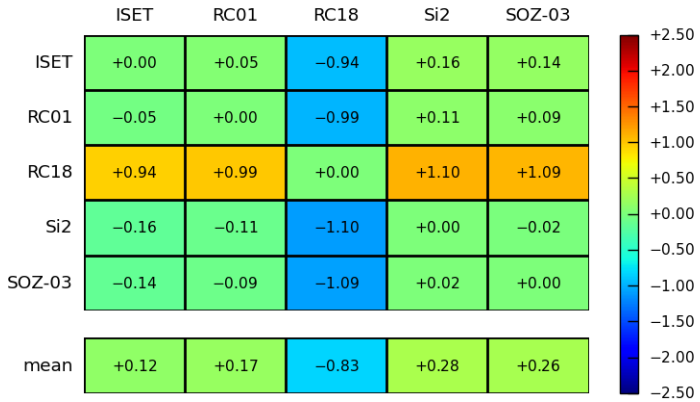

Figure 7. Differences in total energy measured on the single-axis tracker using *field* calibration factors

3.3 Fixed Tilt

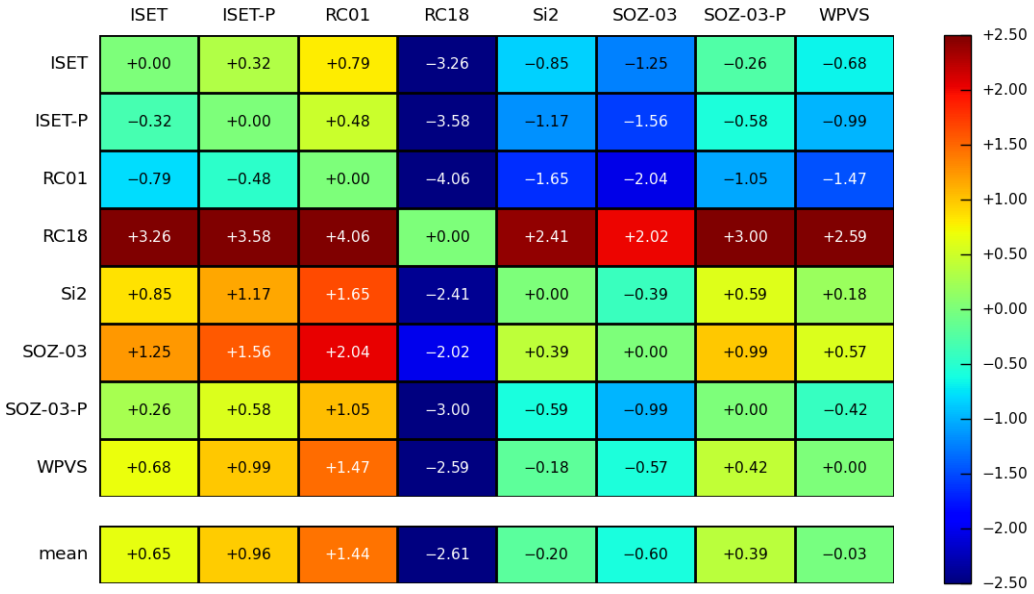

Figure 8. Differences in total energy measured on the fixed-tilt mount using *factory* calibration factors

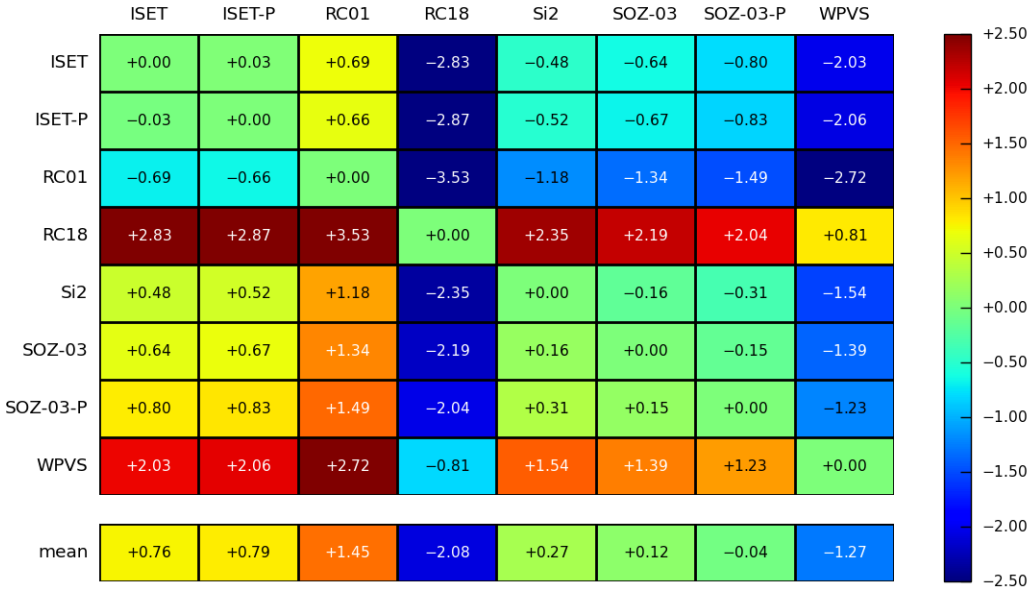

Figure 9. Differences in total energy measured on the fixed-tilt mount using *NREL Cell Lab* calibration factors

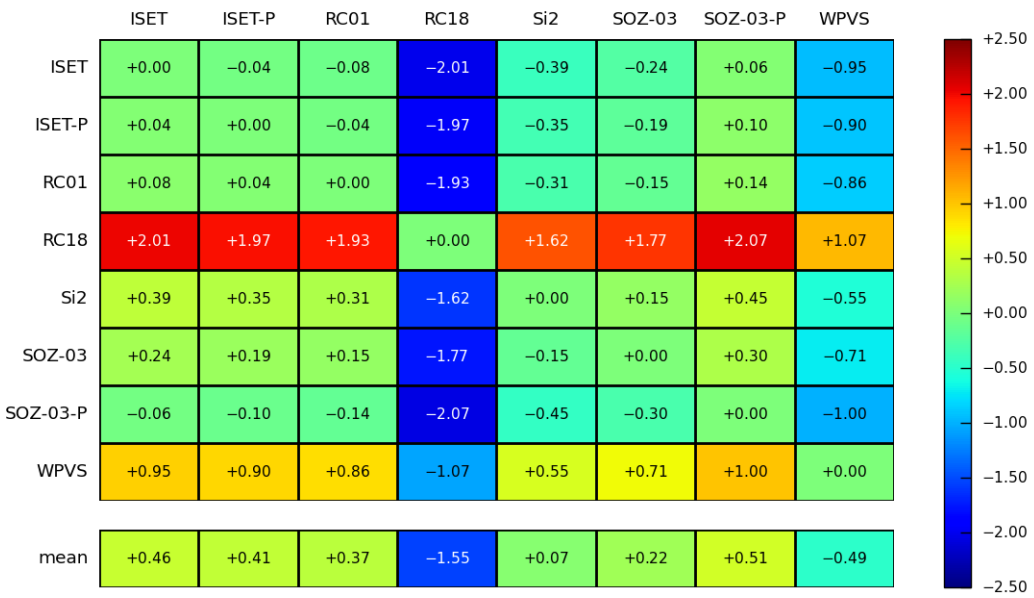

Figure 10. Differences in total energy measured on the fixed-tilt mount using *field* calibration factors

3.4 Observations and Discussion

From the color patterns shown in figures 2–10, two general trends are apparent: First, the consistency among sensors improves when going from the factory calibrations to the Cell Lab calibrations, and it improves further with the field calibrations. Second, the consistency is best on the dual-axis tracker and worst at fixed tilt. These trends are also reflected in the spreads between the highest and lowest measured energy for each case, which are listed in Table 4. Because several cases show a single clear outlier, the spreads are also calculated excluding the most distant outliers, but this does not change the observed trends.

Table 4. Differences between Highest and Lowest Reported Energy in Percentage

The numbers in parenthesis report the differences when the farthest outlier is excluded.

Orientation	Factory Calibration	Cell Lab Calibration	Field Calibration
Dual-axis tracker	2.07 (1.29)	1.80 (1.08)	0.44 (0.21)
Single-axis tracker	3.46 (1.76)	1.96 (1.25)	1.10 (0.14)
Fixed tilt	4.06 (2.04)	3.53 (2.72)	2.07 (1.00)

The improvement in consistency when going from the factory to the Cell Lab calibrations is likely because the procedures, equipment, and reference devices used by the manufacturers differ from each other, whereas NREL used the same for all devices and, further, is capable of the highest levels of accuracy and repeatability. The additional improvement when going to the field calibrations is likely of a more fundamental nature. Cell Lab indoor calibrations use only normal-incidence light, whereas the field calibrations naturally take place in the presence of some diffuse light coming from other directions; thus, for two cells that have the same indoor responsivity, the cell that captures less diffuse light as a result of its directional response would obtain a lower responsivity in the field calibration,

which would lead to higher field irradiance measurements. This effect can be seen with the WPVS cells, both on the dual-axis tracker and at fixed tilt: both report higher annual energy using the field calibration than using the Cell Lab calibration (in relation to any other individual sensor or to their mean). (The directional response of the WPVS cells is further discussed in Section 4.1.) The opposite effect can be seen on the ISET, ISET-P, and RC01 (three left-most columns) in the fixed tilt. Each device has a substantial border with white back sheet material, which boosts sensitivity to light arriving at oblique angles. All three measure lower annual energy with the field calibration than with the Cell Lab calibration (again in relative terms).

The improvement in consistency when going from the Cell Lab to the field calibrations suggests that using calibration reference conditions with a portion of diffuse irradiance would lead to more consistent energy measurements from dissimilar sensors, but such reference conditions could also complicate procedures and traceability. In any case, adapting the reference conditions is only one approach; another approach could be to reduce differences between sensors.

Finally, we observe that even after the field calibration, differences in annual energy remain. Although there could be minor contributions from measurement error and instability, the bulk of these remaining energy differences can be attributed to differences in the sensor characteristics: directional response, spectral response, and others.

Some differences discussed in this section are quite small and could be claimed to lie within the range of calibration and measurement uncertainties. Although this is true, all values are presented and discussed in relative terms, which cancels some shared sources of uncertainty. In any case, this does not change the reality for a PV system owner who might obtain performance ratios varying by 2% or 3% or more, depending on which PV reference cell was purchased.

The observations in this section are not completely new or surprising: The annual energy measurement does not depend only on the calibration factor but also on the measurement conditions and sensor characteristics. Sensors on the single-axis tracker see a range of incidence angles up to nearly 65° (without back tracking), and on the fixed tilt, they range beyond 90°. High incidence angles lead to lower average irradiance levels and lower operating temperatures as well as to a higher proportion of diffuse sky irradiance. Consequently, sensors with differences in linearity, temperature dependency (after nominal correction), or spectral response can potentially produce different annual energy totals. Over the full range of terrestrial climate zones in which PV systems are deployed, the differences are likely to be much larger than shown here for one location. Special applications—for example, measurements on north-facing facades or at the rear side of bifacial systems—will also show higher annual discrepancies because the operating conditions are very different from the calibration conditions. The following section provides insights into these factors by looking at the 1-minute measurements that comprise the annual energy sums.

4 Comparisons of One-Minute Measurements

In this section, the 12 months of measurements are presented in different ways to demonstrate the effect of operating conditions on sensor output. Many differences that are only sometimes evident are much larger than the overall annual differences shown in the previous section. The additional details might be of less concern to a user who is *only* interested in the annual energy of an optimally oriented system, but another user who is planning a short-term acceptance test for a new power plant will be much more motivated to understand these differences.

The purpose of this section is to provide visual evidence of various effects using field data. This is different from characterizing the sensors, which is more easily done using special-purpose testing facilities. This section provides several examples with explanations, and a full catalog of graphs is provided in the 0.

It would be overwhelming to perform detailed comparisons in a pair-wise manner like the previous section; therefore, a reference value is needed for each group. Some possible choices are: a specific sensor, the mean or median value of all sensors, or a theoretical value calculated using spectroradiometer data. If a specific sensor is used as reference, it should be the very best one, but it is not clear which one that would be. The mean value is too strongly influenced by a few large outliers (which do exist), whereas the median value tends to oscillate between a small number of sensors over time as conditions evolve. Finally, a theoretical or modeled value could be the most objective, but there is no standard definition for this (yet). In any case, such a modeled value would also be marked by the uncertainties and imperfections of the instruments that would provide the model inputs, such as the broadband pyranometers and spectroradiometers. The chosen solution is to first apply the field calibrations to align the instrument readings with each other as well as possible. Then, reference values are calculated as a *weighted* mean of the sensor values, where the highest weights are assigned to the sensors that qualitatively have the fewest and smallest deviations during a preliminary comparison with the median.

For all sensors, the deviations from the reference values are calculated as a percentage at every time step (except outliers, as explained in Section 2.2) and presented on two standard graphs: the sun path diagrams and the time charts. For the sun path diagram, the percentage deviations are binned by sun azimuth in 2.5° increments and by sun elevation in 1° increments, and the median value in each bin is coded in color. The color scale is stepped so that a numeric value can be read easily with a precision of 0.5% in the range ±2.5%. (This is the same color scale and range used for the annual energy in the previous section.) The time charts show a colored point for the percentage deviation of every measurement, where the color represents the cell temperature. Their vertical range is expanded to ±10% to show extremes that are hidden from view by the median in the sun path diagram. A complete set of graphs is provided in the appendix, and the following sections explain how certain differences in sensor characteristics can be observed in these graphs.

4.1 Directional Response

Variations in directional response have a minimal effect on the dual-axis tracker and only a moderate effect on the single-axis tracker, where the angle of incidence (AOI) reaches a peak near 63° at noon in winter. On the fixed-tilt system, on the other hand, the angles exceed 90° in summer, and some important differences appear. In the sun path diagrams that follow, the limits of the field of view of the

tilted cells (AOI = 90°) are drawn with a double line. The other double line is the geographic horizon, showing mountains to the south and west.

The sun path diagram in Figure 11 shows IMT Si2, which has a very abrupt drop in response just before the sun reaches the limits of the theoretical field of view. The cause for this appears to be the raised edge of the enclosure that partly shades the cell at very high incidence angles.

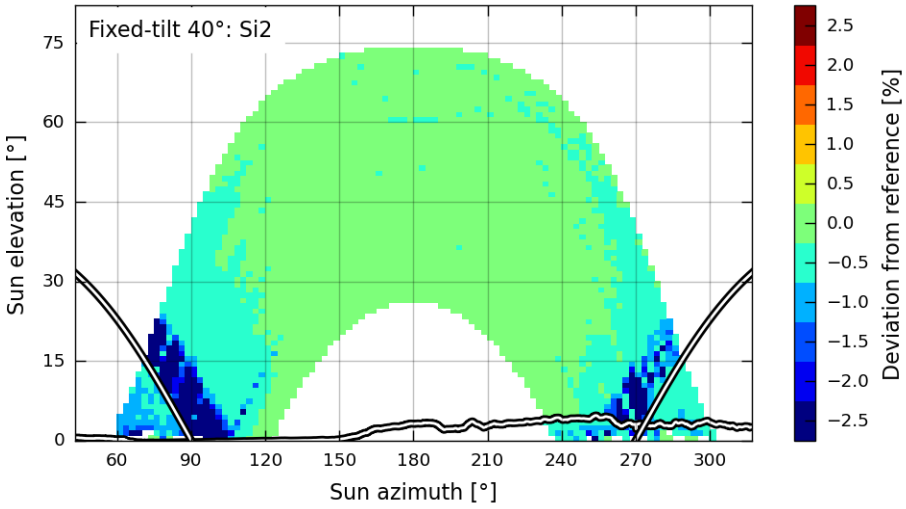

Figure 11. Abrupt drop in response with increasing AOI probably caused by the raised edge on IMT Si2

Figure 12 shows a very different pattern, with substantial asymmetry. The EETS RC01 has an enhanced response in the morning, especially near the limits of the field of view, whereas in the evening, its response is somewhat lower than the reference.

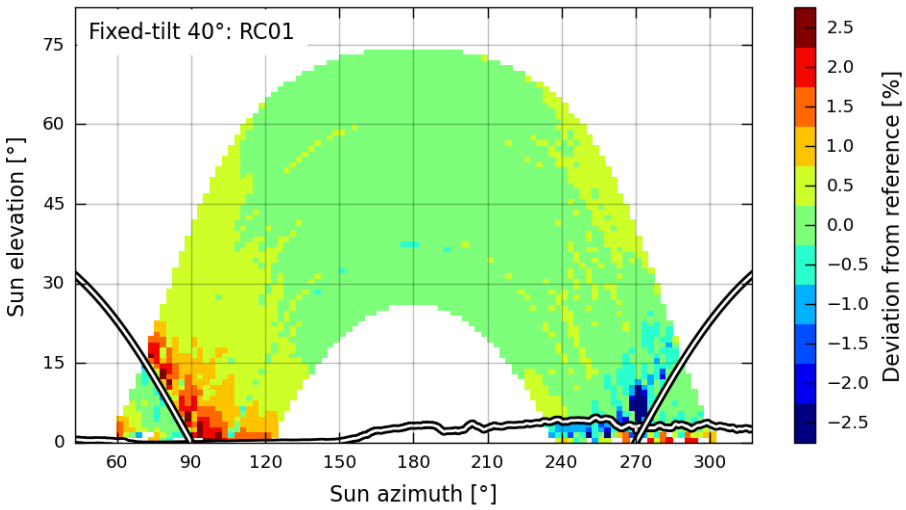

Figure 12. Asymmetric response at high incidence angles probably caused by the white border on EETS RC01

This asymmetric deviation results from the asymmetric physical construction of the sensor. The RC01 consists of two half-cells to measure I_{sc} and V_{oc}, for irradiance and temperature, respectively. When the unit is mounted with the two halves oriented side by side (as is commonly done based on the markings

on the device), the half-cell that measures irradiance is located on the west side, and Figure 12 shows that it receives an irradiance boost at high incidence angles from the east. The likely explanation for this is that some light entering the glass in the V_{oc} half is transported via internal reflections to the I_{sc} half. A similar effect was recently observed in full-size modules, where each cell in the module was measured separately during an AOI response test (Coston et al. 2021). The small reduction at high incidence angles from the west can be attributed to the raised edge of the frame. In relation to the cell area, this frame represents less of an obstacle than the raised edge of the IMT (Figure 11).

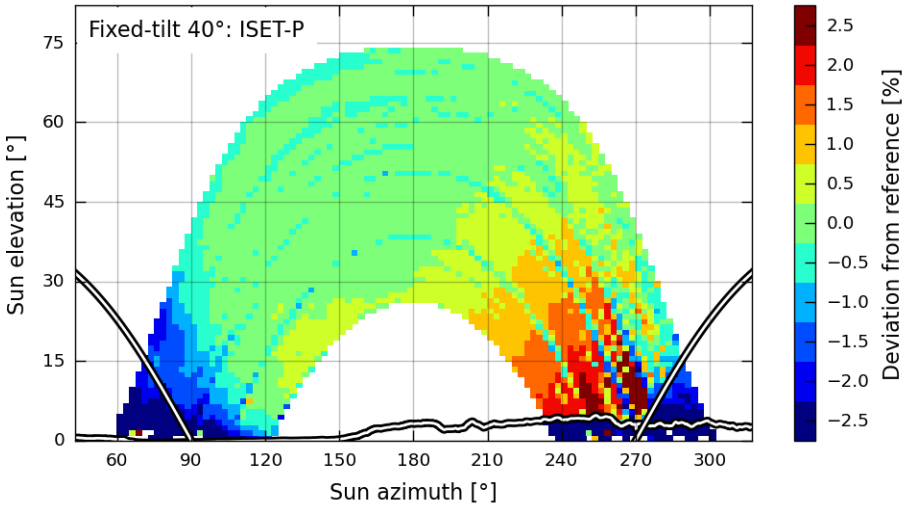

Figure 13. Asymmetrical response of the IKS ISET-P cell presumed to be caused by alignment error

The ISET-P polycrystalline cell (Figure 13) also shows a substantially asymmetric response in the fixed-tilt orientation. The sensor itself has no apparent structural asymmetry, but a qualitative examination of the unit found that it was mounted with a slight westward tilt. This would be a plausible explanation for the observation, and it illustrates how accurate alignment is both important and difficult.

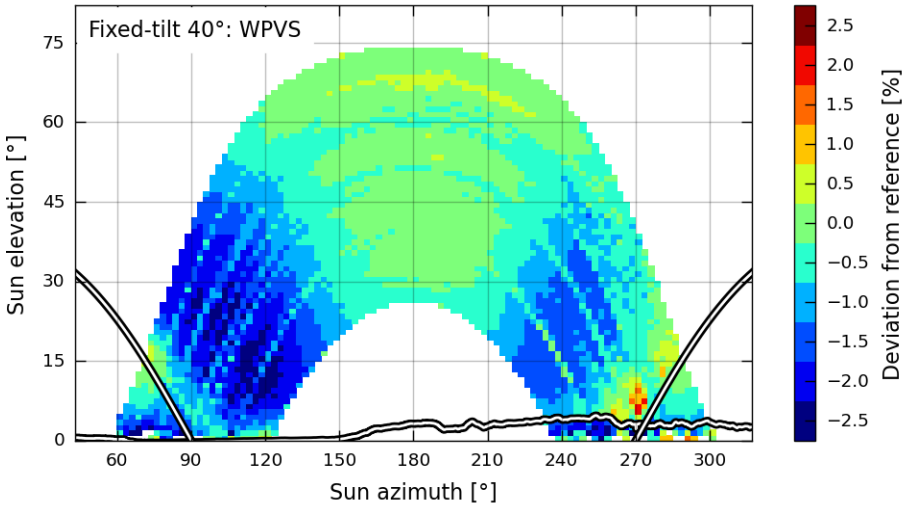

Figure 14. Overall directional response of the Fraunhofer WPVS

Finally, the WPVS cell shows a gradual reduction in the measured irradiance with increasing incidence angle. The fact that there is a recovery as the AOI approaches and exceeds 90° (at the double line) confirms that this is a directional response characteristic. At those angles, the measured irradiance is primarily diffuse and therefore less affected.

4.2 Nonlinearity or Offset Error

As shown in Section 3, the Atonometrics RC18 measures lower annual energy than all other sensors in all three orientations but especially at fixed tilt. The sun path diagram in Figure 15 shows that the underestimation occurs primarily at lower sun incidence angles. Unlike the WPVS in Figure 14, however, the underestimation persists when the sun is behind the plane of the cell, suggesting that this is not primarily related to directional response but rather to irradiance intensity: The largest relative errors occur at the lowest irradiance levels. Figure 16 shows this more clearly by plotting the percentage deviations against irradiance intensity. This is the typical signature of a negative offset error, which is a form of nonlinearity because output is no longer linearly proportional to irradiance.

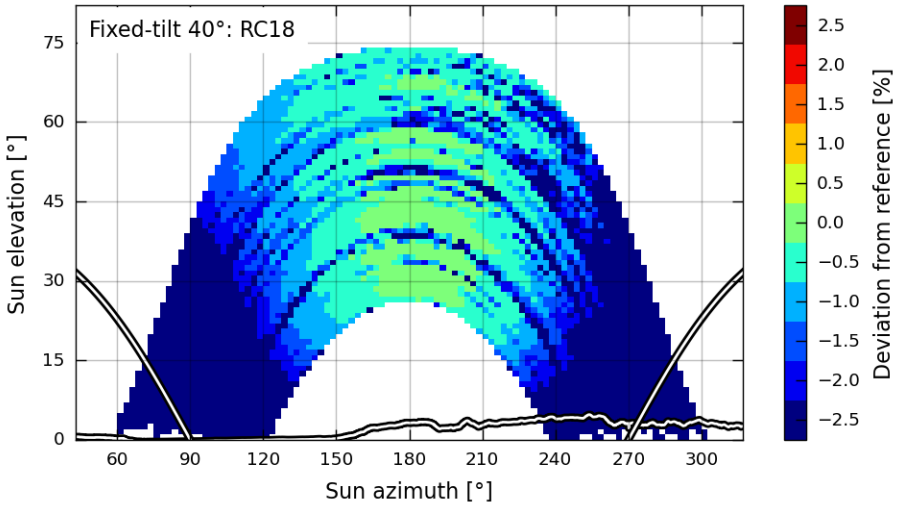

Figure 15. Underestimation under low irradiance conditions by the Atonometrics RC18

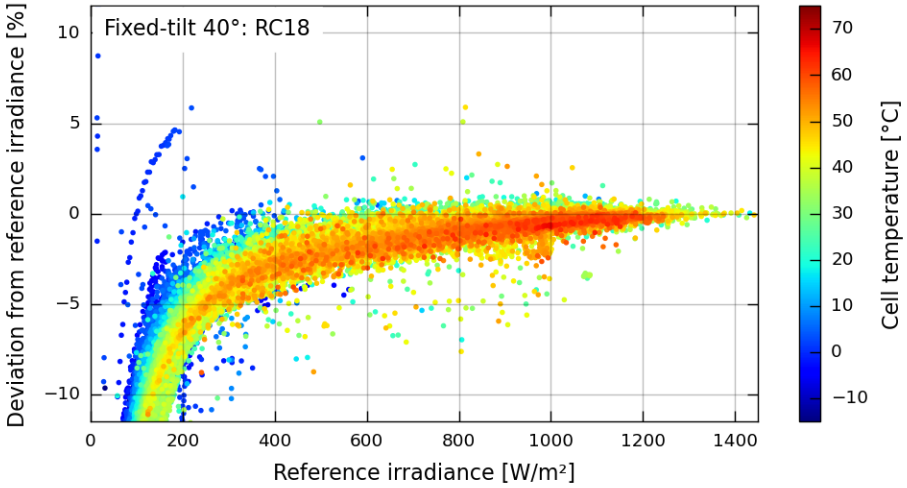

Figure 16. Deviation from reference irradiance versus irradiance intensity for the Atonometrics RC18

As discussed in Section 2.2, we already identified and corrected for offset errors in the data acquisition system related to the RC18 analog output. The deviations observed here are larger and could be evidence of an offset in the measurement electronics of the RC18. Indeed, after SRRL began to record digital values on 2022-01-18, we observe that the digital I_{sc} values at night usually range from −8 to −12 mV (equivalent to approximately −8 to −12 W/m^2). Both the calculated irradiance available digitally via Modbus and the analog output signals are derived from the internal I_{sc} measurement, thus all outputs are affected by this internal offset.

Although the impact of these internal offsets on both the analog and digital irradiance measurements is substantial, it should also be relatively easy for the manufacturer to fix by using a two-point (offset/gain) calibration, perhaps requiring a software update.

4.3 Spectral Response

The spectral responses of all the reference cells were measured at the NREL Cell Lab as part of the initial calibration, and they are shown in Figure 17. The WPVS cells stand out as having a response that extends furthers into the ultraviolet regions as well as into the infrared, and the ISET (monocrystalline) cell surprises with its very low infrared response. Another interesting aspect of these measurements is that for the ISET-P polycrystalline cell, the spectral response is quite similar to most of the monocrystalline cells; and the spectral response of the SOZ-03-P polycrystalline cell supplied by NES is virtually indistinguishable from its monocrystalline sibling, the SOZ-03.

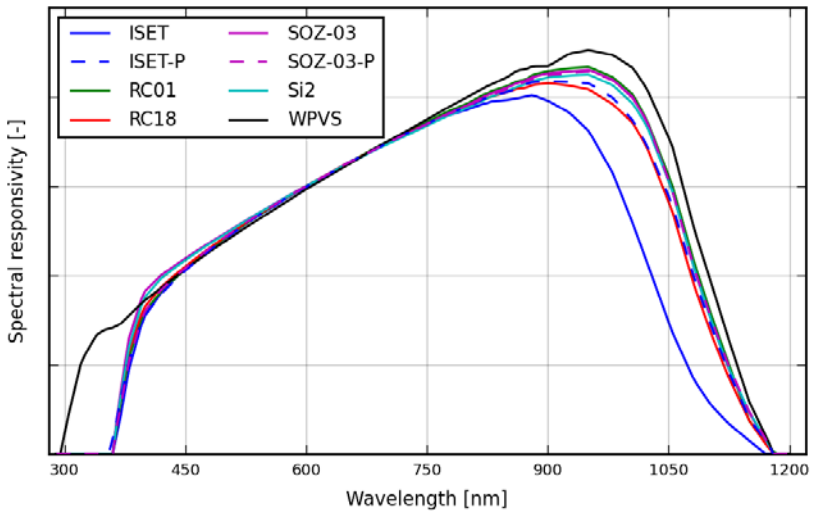

Figure 17. Relative spectral responses measured by the NREL Cell Lab

The two outliers for spectral response can be spotted easily from the sun path diagrams for the dual-axis tracker where directional response effects are minimal. As shown in Figure 18, the WPVS picks up a much higher proportion of the reddish beam irradiance in the very early morning than the reference. In the late evening, the difference from the reference is much smaller because the mountains block that reddish beam irradiance. As expected, the opposite trend is shown for the ISET cell in Figure 19.

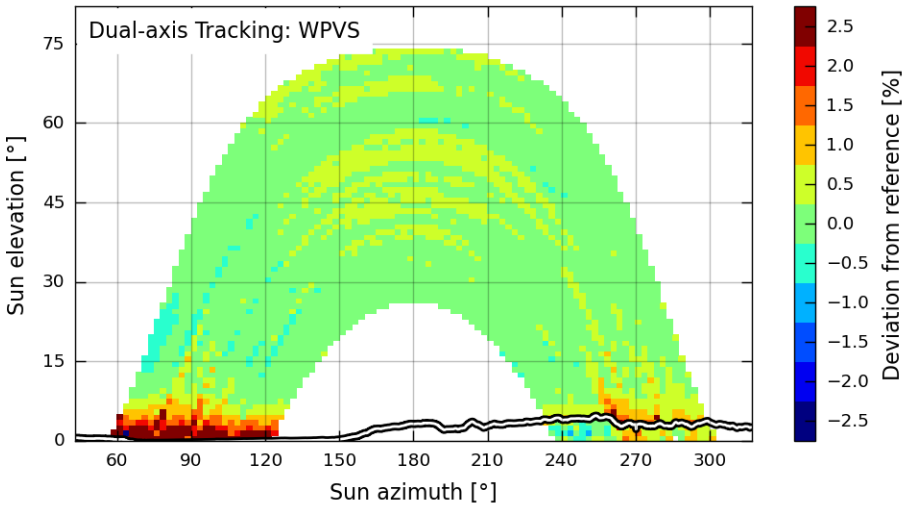

Figure 18. Effect of strong infrared spectral response of the Fraunhofer WPVS cell

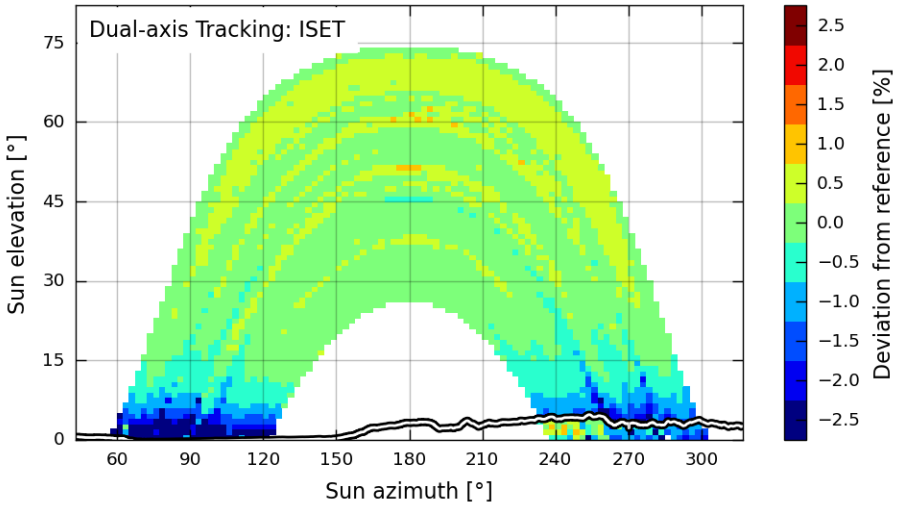

Figure 19. Effect of weak infrared response of the IKS ISET cell

These observations are corroborated by spectral mismatch calculations using the measured spectral response and the measured spectra. The morning values for the monocrystalline cells on the dual-axis tracker are shown in Figure 20. Note that none of these spectral responses are inherently bad; but any of them can be bad choices if they differ substantially from the PV module or system they are to be used with. Figure 20 thus illustrates some possible measurement error scenarios that could result from not knowing the spectral response of either the sensor or the module.

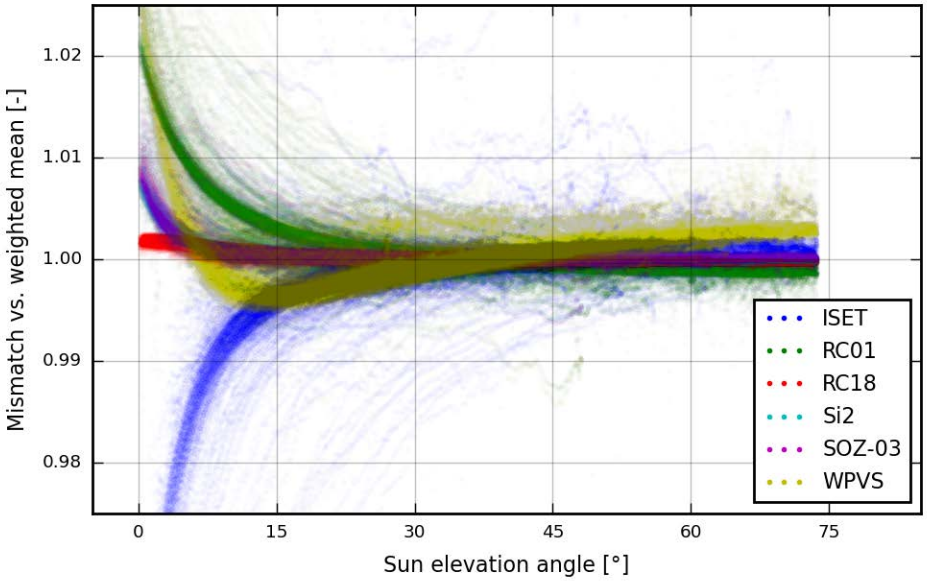

Figure 20. Differences in calculated spectral mismatch between monocrystalline cells on the dual-axis tracker

4.4 Temperature Response

Differences in temperature response are somewhat difficult to detect in the sun path diagrams but not impossible. Because each irradiance signal is already temperature compensated (see Section 2.2), the diagrams potentially show whether a signal was overcompensated or undercompensated with respect to the reference. The NES polycrystalline cell (SOZ-03-P) has been compensated using the factory-recommended value of 600 ppm, whereas the NREL Cell Lab determined values of 440 and 435 ppm for two cells of this type; therefore, the measurements are overcompensated. Field calibration occurred at high irradiance and high temperature, so the overcompensation shown in in Figure 21 appears as higher irradiance readings when the cell is cold.

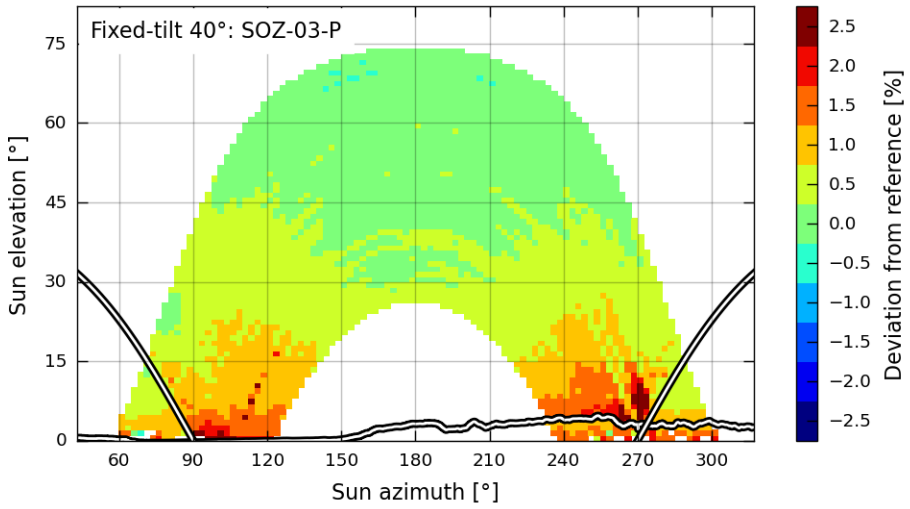

Figure 21. Factory-recommended temperature coefficient of 600ppm leads to overcompensation and larger deviations away from the field calibration conditions.

Temperature coefficients will, no doubt, be further analyzed in a future report, but the absolute operating temperatures are also of interest. These are therefore illustrated in the time-series diagrams of the appendix. Once again, the WPVS cell (Figure 22) is an outlier because it runs substantially cooler than that of the others. This offers a small advantage by needing smaller temperature corrections and a potentially larger advantage in terms of long-term stability and service life. Stability is another aspect that will be monitored and analyzed in future reports.

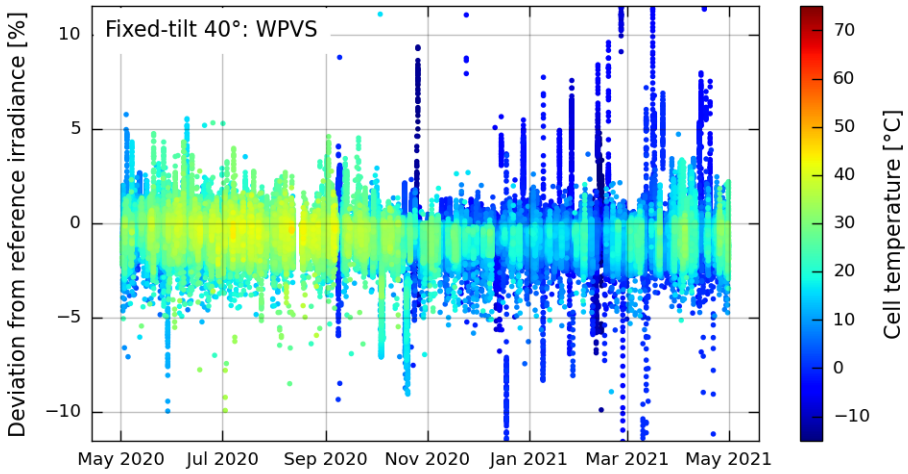

Figure 22. Time series showing comparatively low operating temperatures for the WPVS cell

4.5 Annual Distribution of Deviations

Finally, the deviations from the reference irradiance discussed in this chapter are summarized by instrument in Figure 23, Figure 24, and Figure 25. Each segment of the colored bars represents a fraction of the number of readings during the year, and the black lines identify the median error values. The two lighter-colored sections together represent 68% of the readings, and together with two darker sections, they cover 95% of the readings. These quantiles are chosen to coincide with typical uncertainty coverage factors k = 1 and k = 2, respectively.

The median deviations from the reference irradiance shown in these graphs are quite similar to the deviations from the mean total annual energy shown in Section 3 using the field calibration factors. The bars summarize the variability of the deviations on individual measurements. This variability is not affected by the calibration factors but is solely a function of the instrument characteristics. If the reference irradiance is considered to be the best estimate or the "true" value of the quantity to be measured, then the model showing the lowest variability in these figures is the one that has done the best job measuring it.

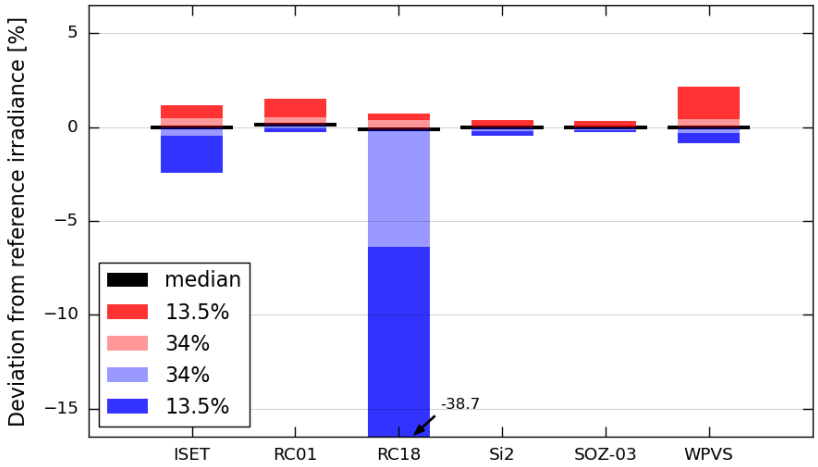

Figure 23. Distribution of percentage errors for each instrument on the dual-axis tracker.

Each segment of the colored bars represents a fraction of the number of readings during the year, and the black lines identify the median error values. The two lighter-colored sections together represent 68% of the readings, and together with two darker sections, they cover 95% of the readings.

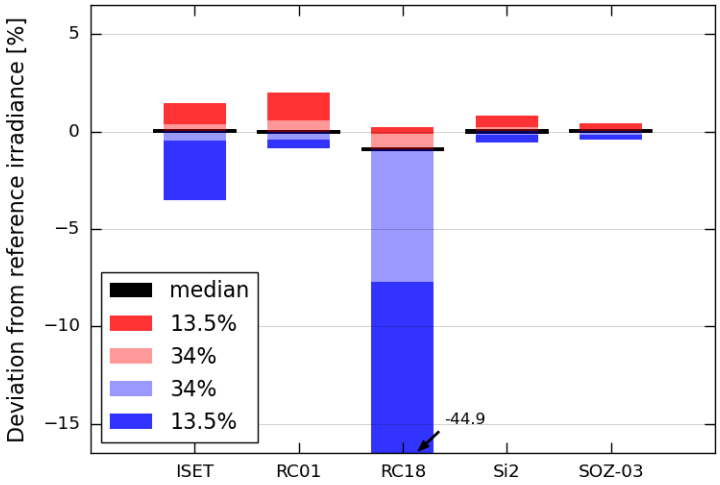

Figure 24. Distribution of percentage errors for each instrument on the single-axis tracker.

(See notes in Figure 23.)

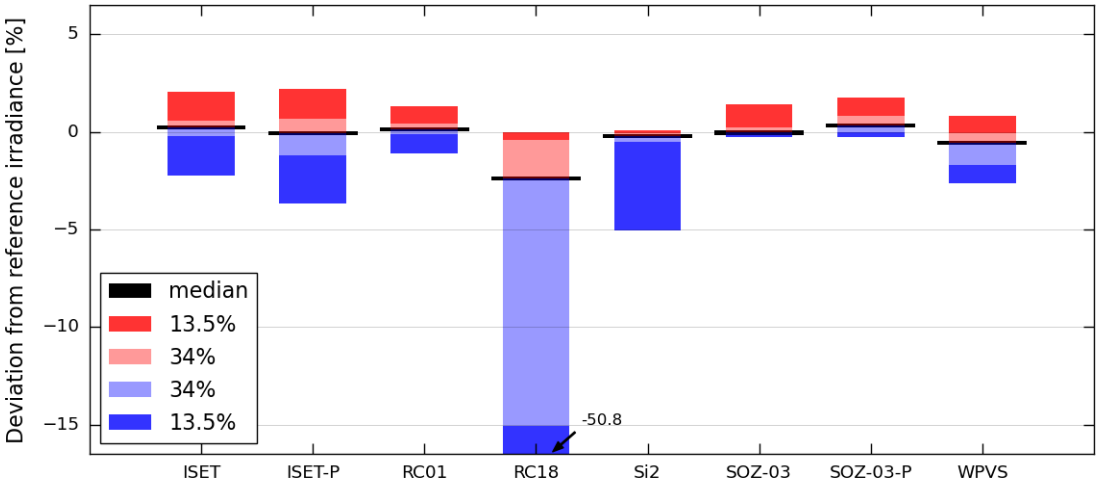

Figure 25. Distribution of percentage errors for each instrument at fixed tilt.

(See notes in Figure 23.)

5 Summary and Conclusions

One year of monitoring different types of reference cells in three different orientations at SRRL has yielded a rich data set for analysis. This report compares the annual energy measured by different sensors and looks deeper into differences that vary with time and sun position. In addition to the examples discussed in the text, a full catalog of visual results is provided in the appendix.

Measured annual energy depends directly on calibration factors, and it is demonstrated that better agreement among the sensors is achieved when all sensors are calibrated by one laboratory using one method rather than using the factory calibration factors. The best agreement among sensors is obtained using a field calibration for each group having a different orientation. The bulk of the remaining energy differences can be attributed to differences in the sensor characteristics: directional response, spectral response, and others.

The differences in annual energy measured at SRRL are not very large when viewed in relation to other irradiance measurement uncertainties, such as soiling, to name just one; hence, some might argue that no improvement is necessary. But there are three additional factors to consider: First, the magnitudes of the annual differences will vary by location and climate. Second, there are important use cases that require accurate readings for time intervals much shorter than 1 year, such as capacity testing. Third, differences may be accentuated for deployment in atypical conditions, such on vertical facades or the back side of bifacial systems. The latter, in particular, requires accuracy at low irradiance, which was found lacking in one of the products.

Overall, the analysis of differences in measured irradiance on shorter timescales yields evidence of substantial differences in directional response, which highlights the need to standardize this characteristic of reference cells. The spectral responses of the mono- and polycrystalline devices were also found to vary. This does not pose a problem for calibration as long as the spectral irradiance can be measured to calculate the spectral mismatch factor; however, the variety of responses shown here calls into question the often tacit assumption that any monocrystalline reference cell is adequately matched to any monocrystalline PV system in field applications. Also notable is the fact that there is no clear separation between monocrystalline and polycrystalline spectral responses in this set of reference cell products.

To conclude that commercial PV reference cells have their differences would merely state the obvious. The consequence of these differences is higher uncertainty about the quantity being measured, which, in turn, reduces the usability and usefulness of these devices in outdoor applications. For commercial PV reference cells to reach their full potential as accurate outdoor reference devices, their target characteristics should be more completely specified. This could take the form of a unique definition (as for pyranometers), but more likely one or two degrees of freedom will be needed to accommodate different PV technologies. Such definitions would give manufacturers of reference devices clear objectives to pursue, and would give users clear criteria to compare products and interpret measurements.

References

ASTM. 2015. "ASTM E1362-15 Test Methods for Calibration of Non-Concentrator Photovoltaic Non-Primary Reference Cells." ASTM International. https://doi.org/10.1520/E1362-15.

Coston, Joseph, Charles Robinson, Bruce King, Jennifer Braid, Dan Riley, and Joshua S. Stein. 2021. "Effects of Solar Angle of Incidence on Intramodular Photovoltaic Irradiance Uniformity." In *2021 IEEE 48th Photovoltaic Specialists Conference (PVSC)*, 1499–1503. Fort Lauderdale, FL, USA: IEEE. https://doi.org/10.1109/PVSC43889.2021.9518595.

Driesse, Anton. 2021. "PV Reference Cells for Outdoor Use: An Investigation of Calibration Factors." NREL/SR-5D00-80437. National Renewable Energy Lab. (NREL), Golden, CO (United States). https://doi.org/10.2172/1823768.

Driesse, Anton, and Wim Zaaiman. 2015. "Characterization of Global Irradiance Sensors for Use with PV Systems." In *2015 IEEE 42nd Photovoltaic Specialist Conference (PVSC)*, 1–5. New Orleans, LA: IEEE. https://doi.org/10.1109/PVSC.2015.7356004.

IEC. 2015. "IEC 60904-2: Photovoltaic Devices – Part 2: Requirements for Photovoltaic Reference Devices." Third edition. Geneva: IEC.

Stoffel, T., and A. Andreas. 1981. "NREL Solar Radiation Research Laboratory (SRRL): Baseline Measurement System (BMS); Golden, Colorado (Data)." Not Available. https://doi.org/10.5439/1052221.

Vignola, Frank, Josh Peterson, Richard Kessler, Vikram Sandhu, Sean Snider, Aron Habte, Peter Gotseff, Afshin Andreas, Manajit Sengupta, and Fotis Mavromatakis. 2021. "Improved Field Evaluation of Reference Cells Using Spectral Measurements." *Solar Energy* 215 (February): 482–91. https://doi.org/10.1016/j.solener.2020.12.063.

Appendix. Graphic Results for Each Instrument

The following pages provide detailed graphics for each instrument model and each mounting orientation. Further explanations about the design of the graphs are found in Section 4.

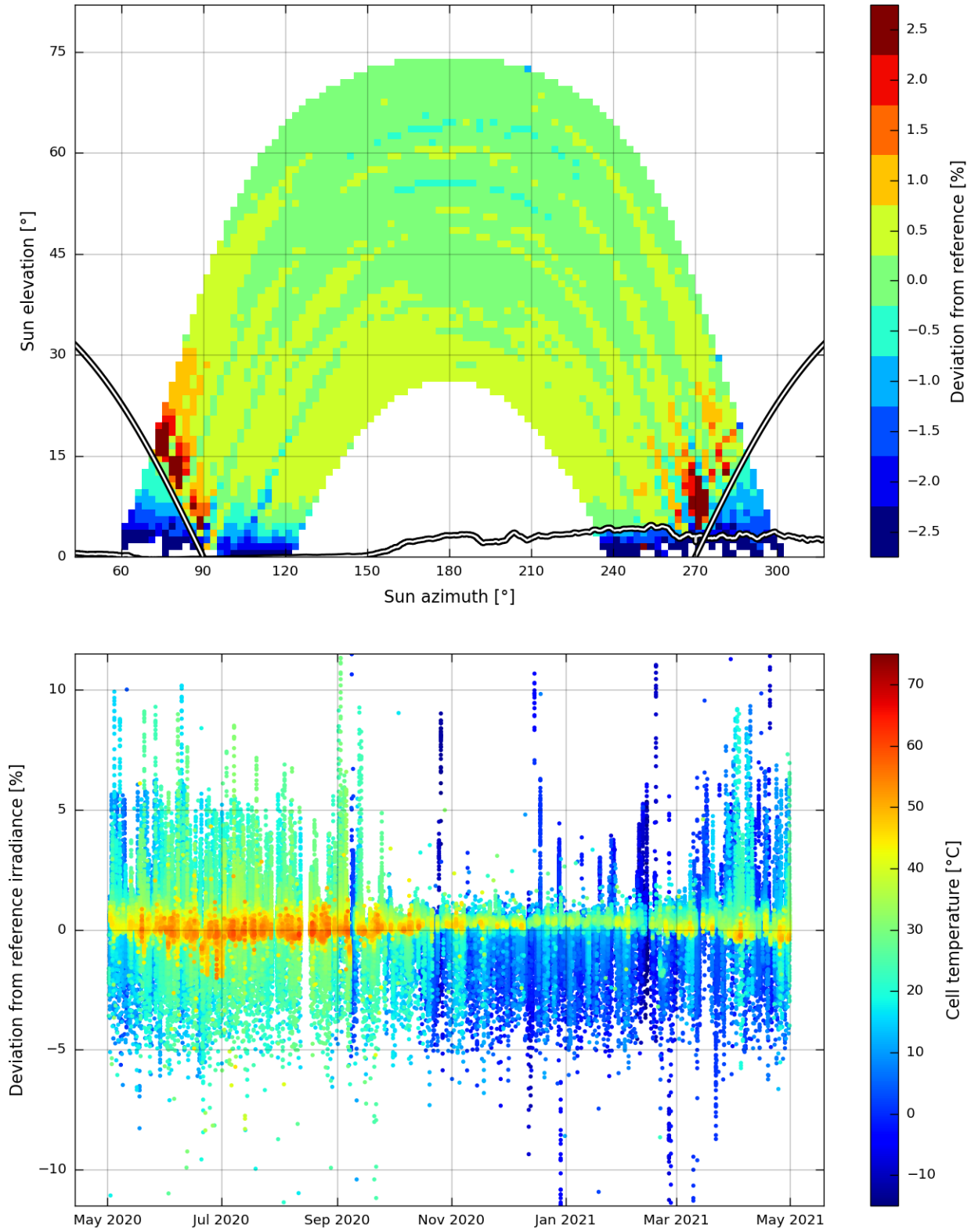

Figure A-1 Detailed results for model ISET, fixed-tilt 40°.

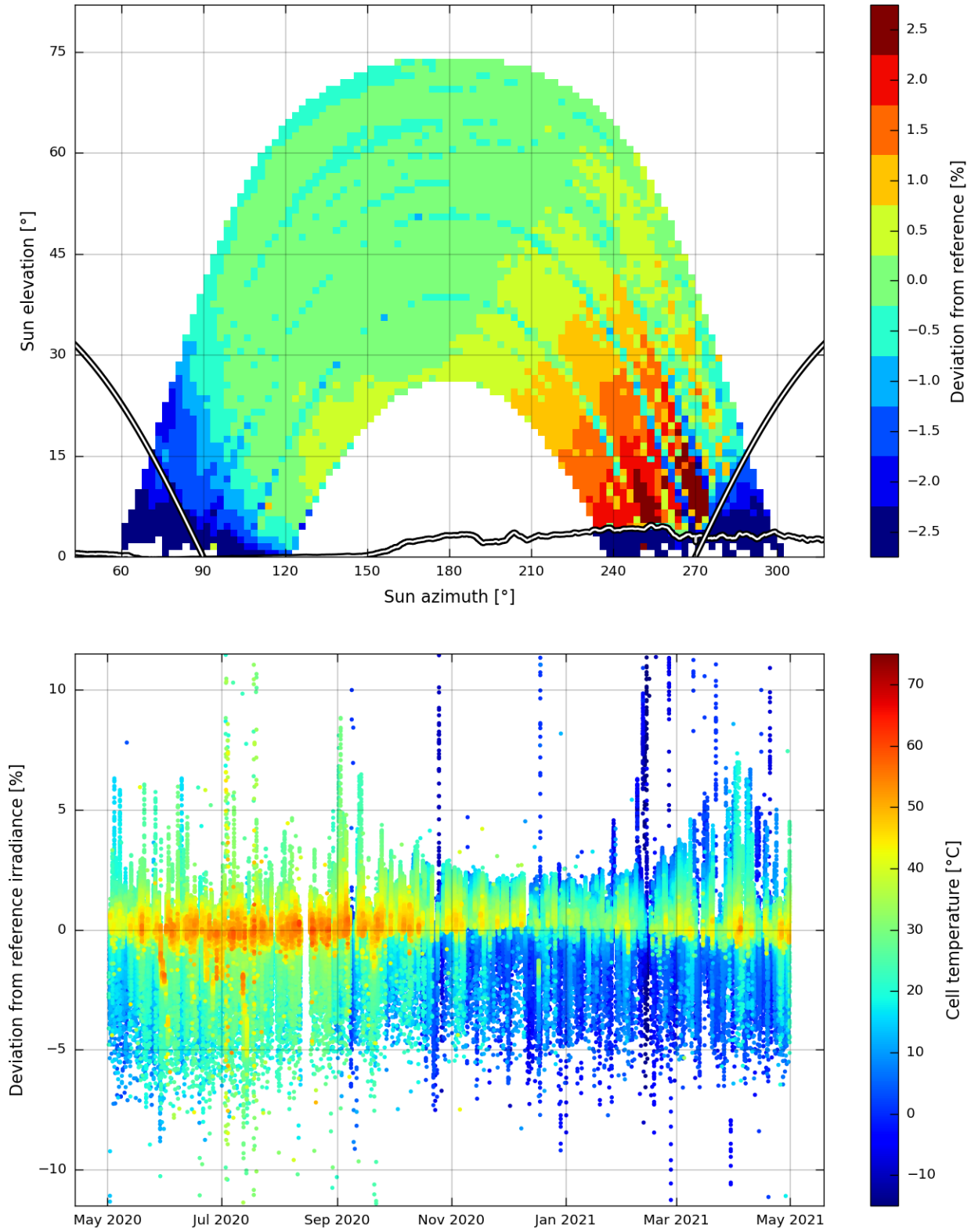

Figure A-2 Detailed results for model ISET-P, fixed-tilt 40°.

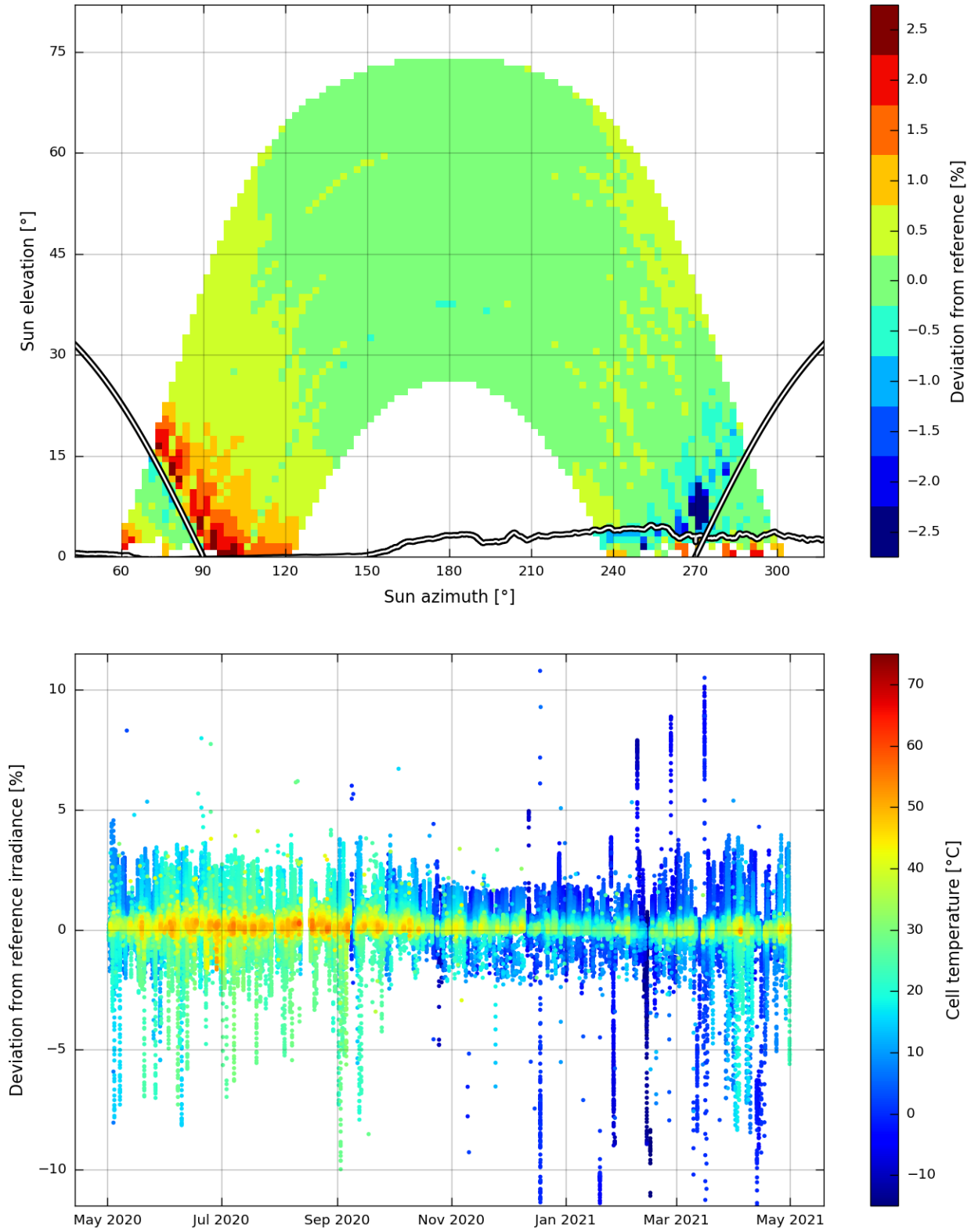

Figure A-3 Detailed results for model RC01, fixed-tilt 40°.

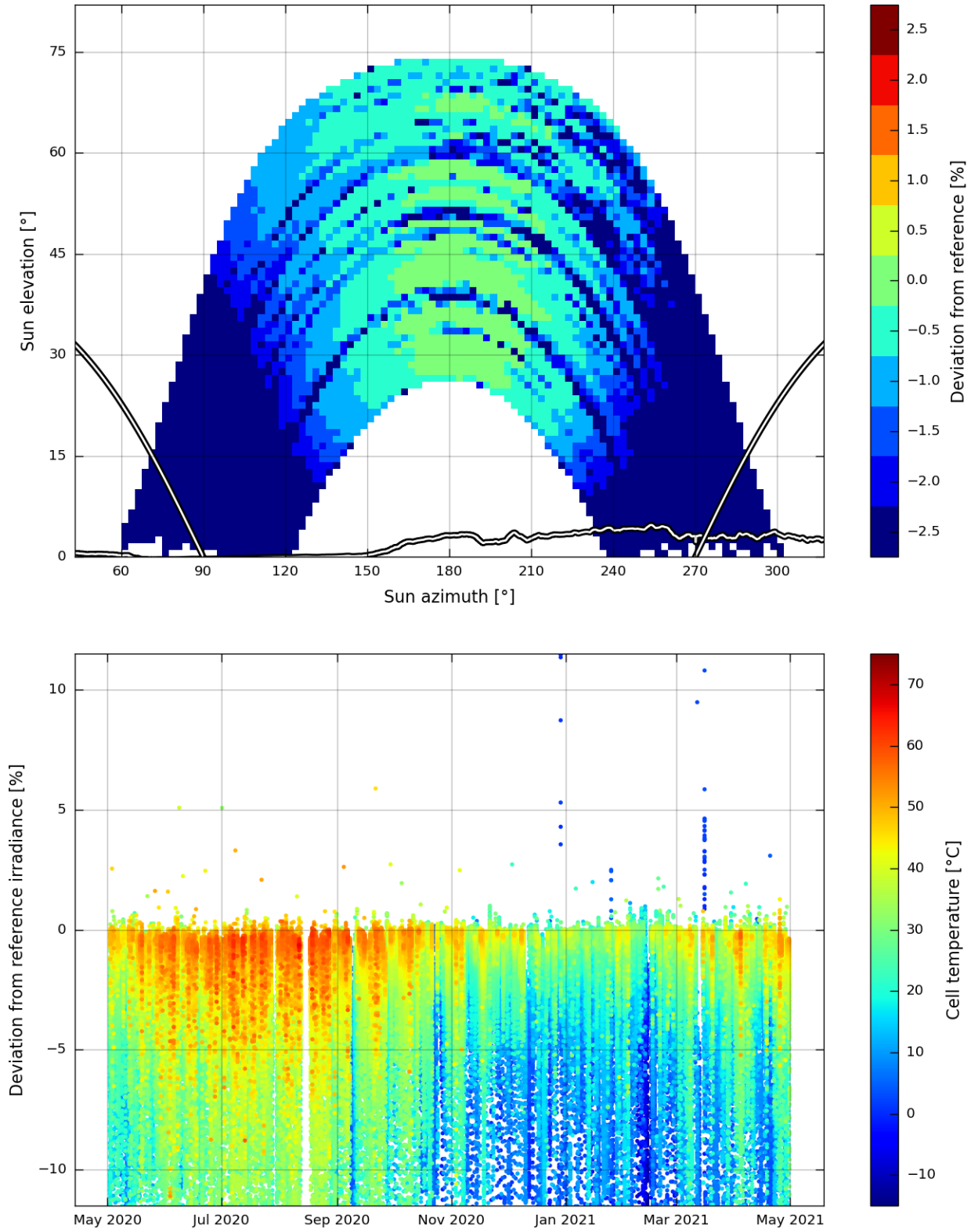

Figure A-4 Detailed results for model RC18, fixed-tilt 40°.

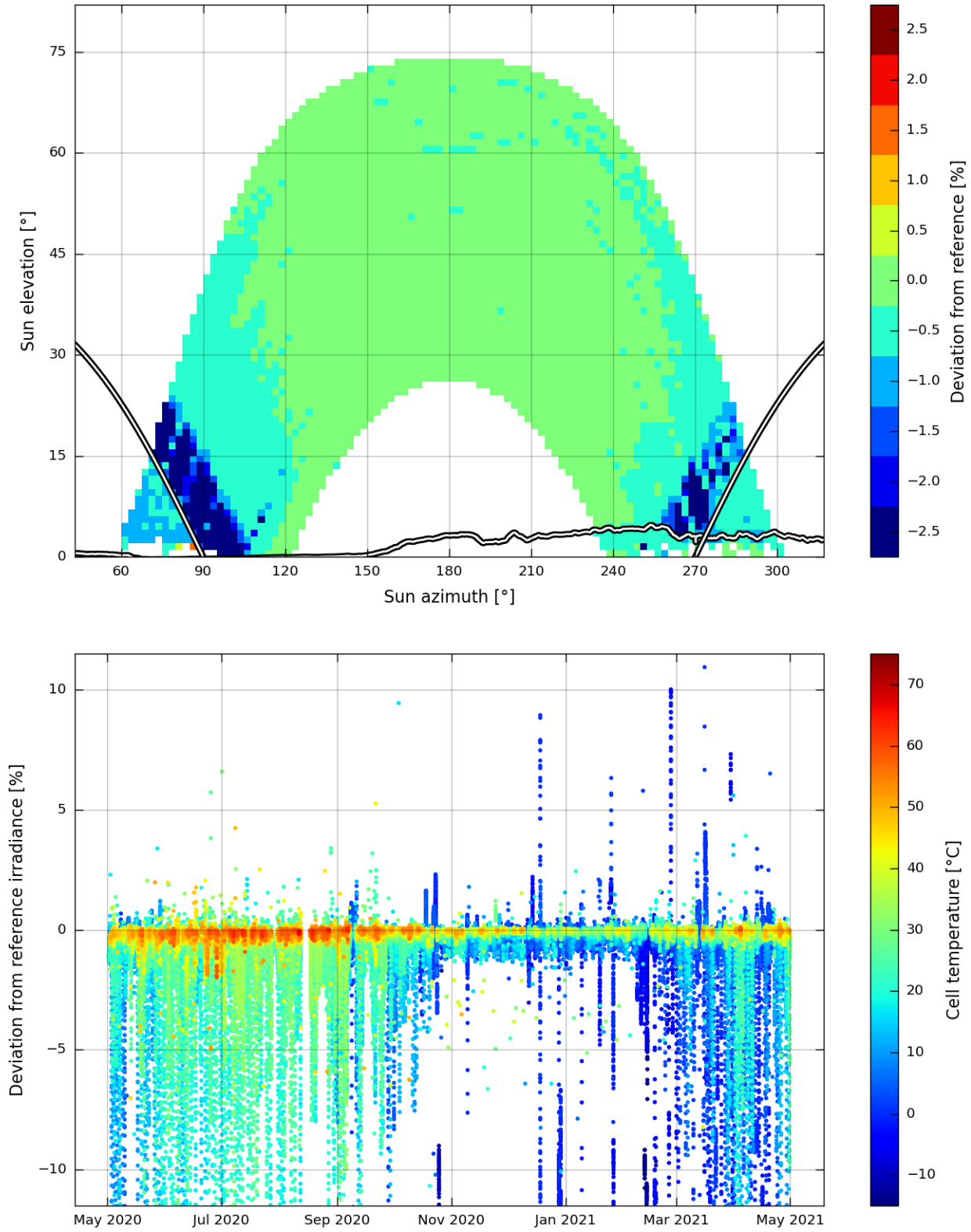

Figure A-5 Detailed results for model Si2, fixed-tilt 40°.

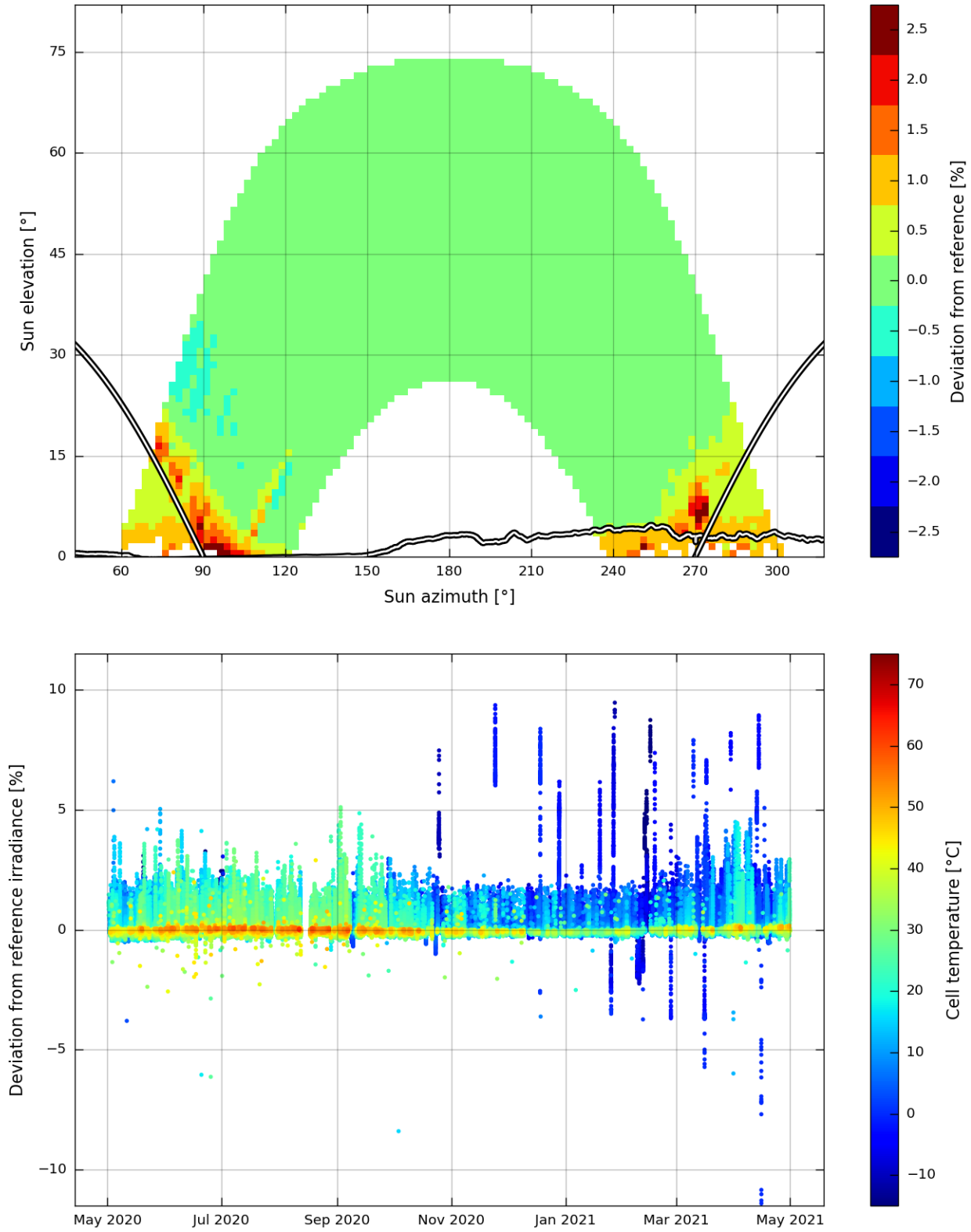

Figure A-6 Detailed results for model SOZ-03, fixed-tilt 40°.

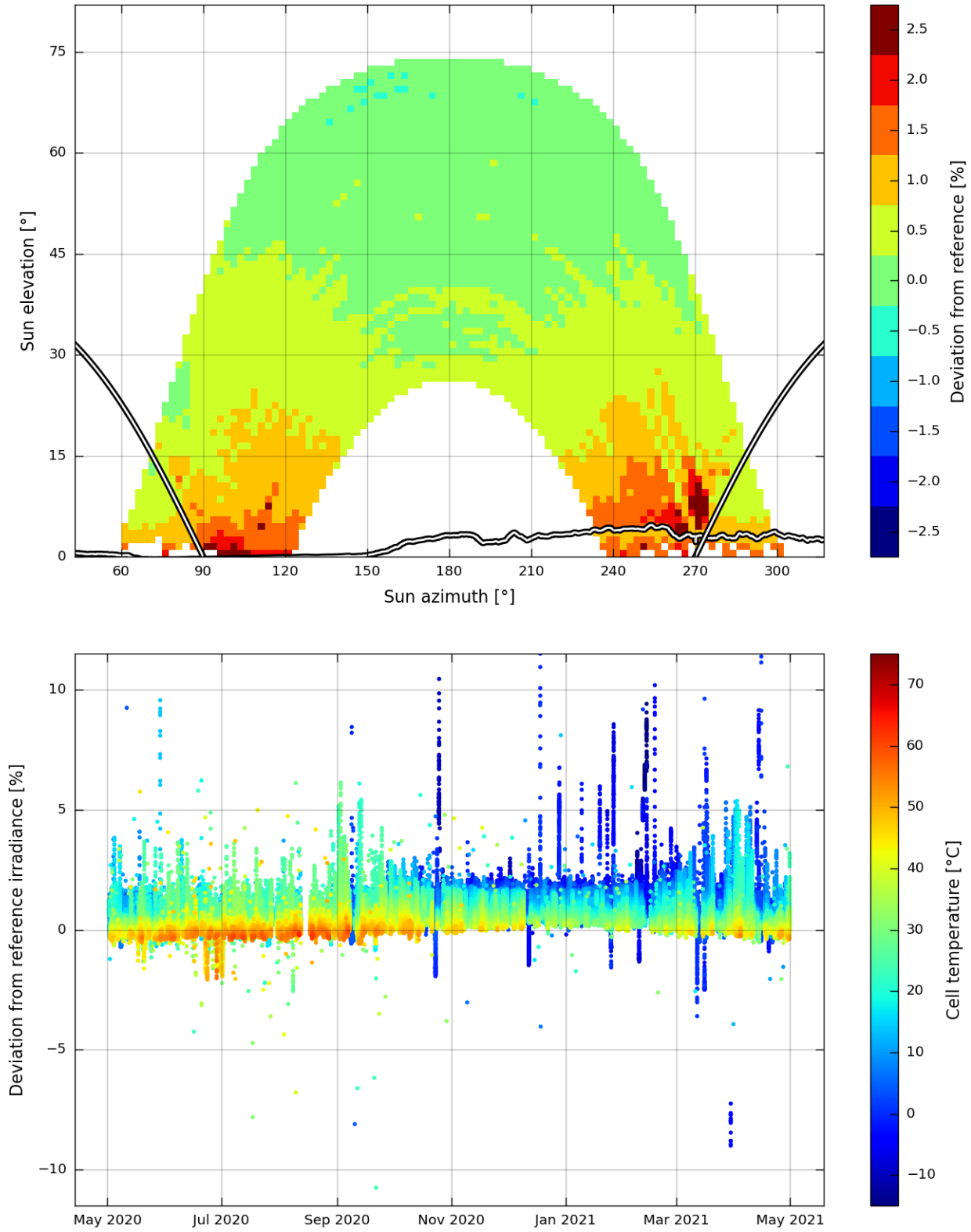

Figure A-7 Detailed results for model SOZ-03-P, fixed-tilt 40°.

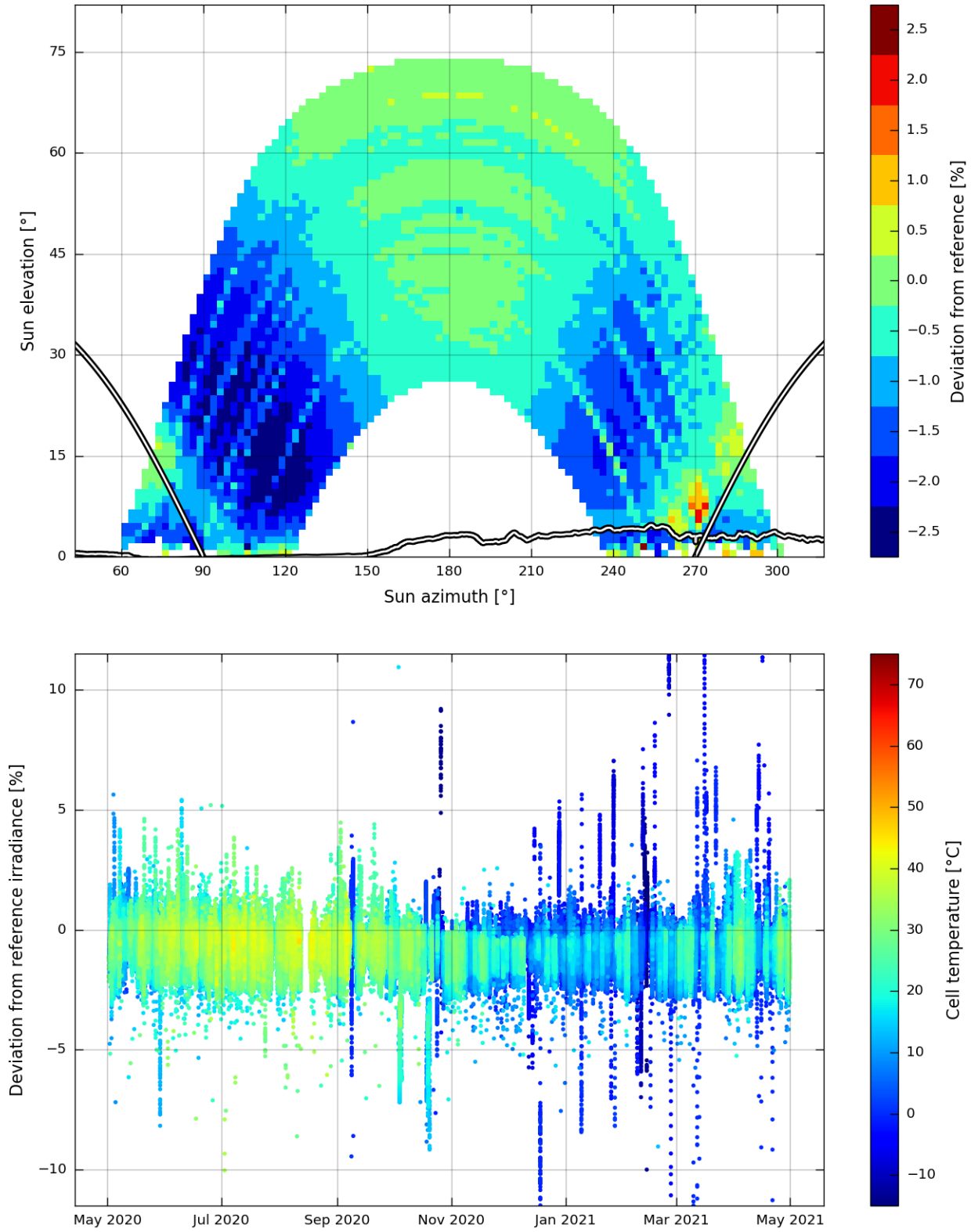

Figure A-8 Detailed results for model WPVS, fixed-tilt 40°.

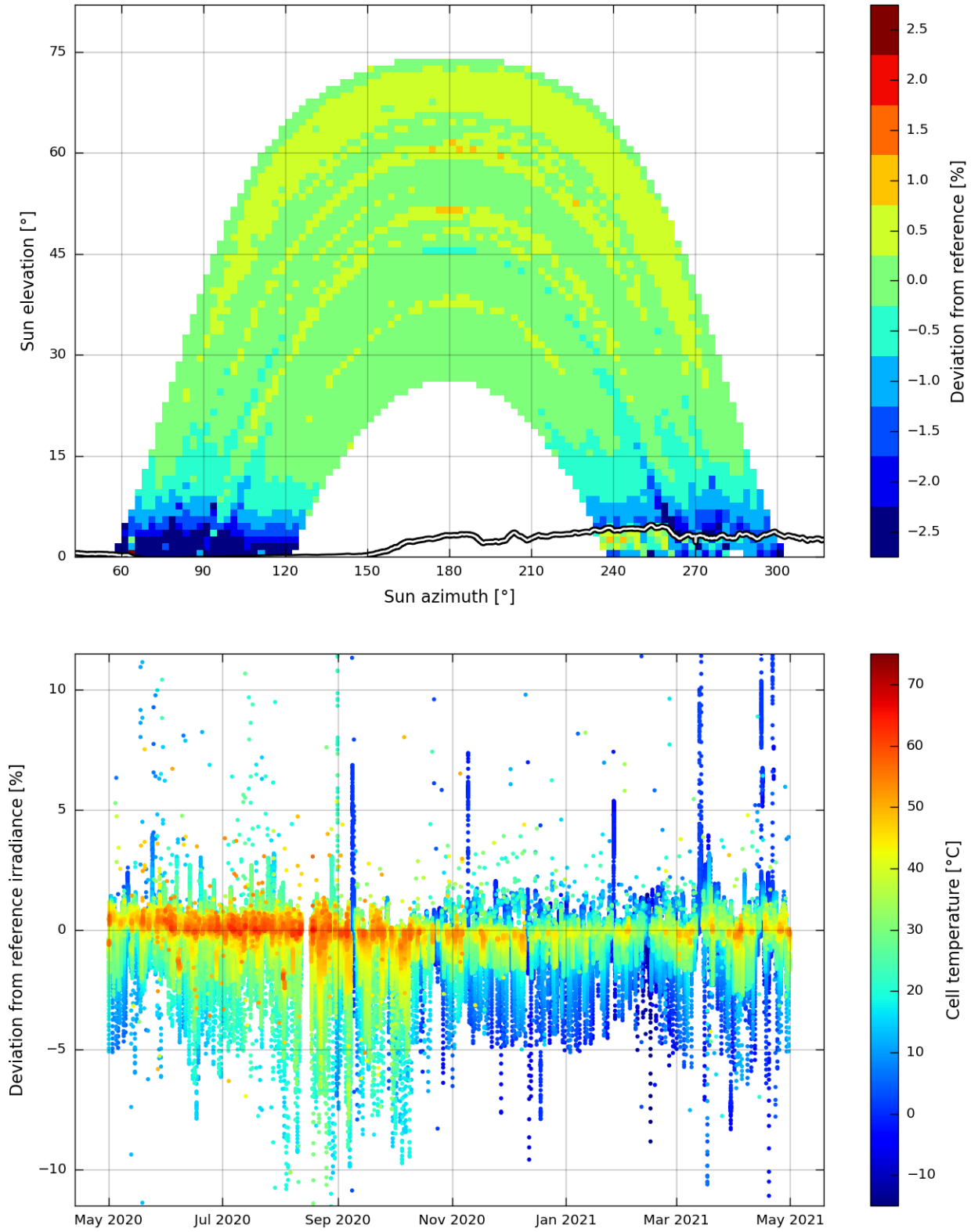

Figure A-9 Detailed results for model ISET, dual-axis tracker.

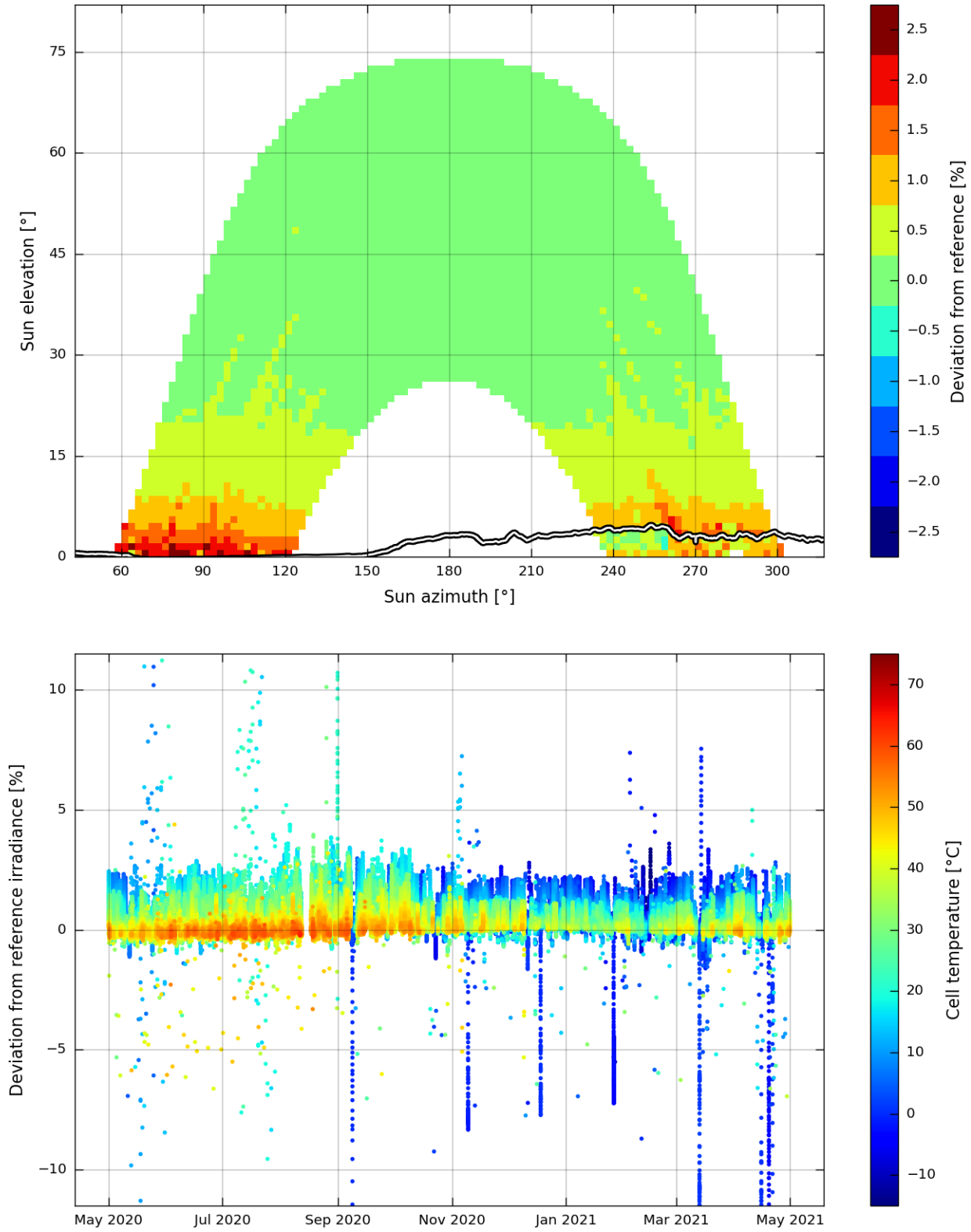

Figure A-10 Detailed results for model RC01, dual-axis tracker.

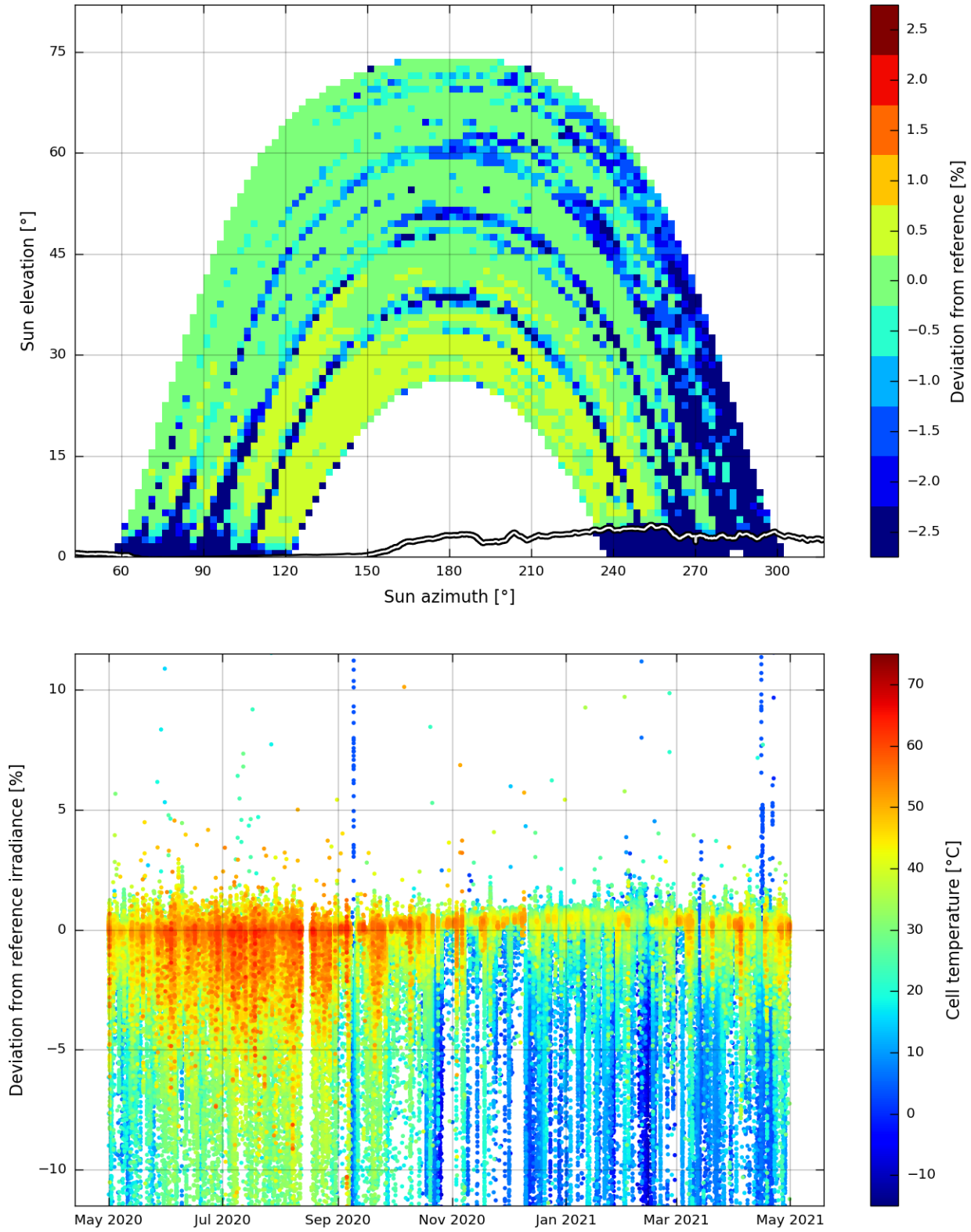

Figure A-11 Detailed results for model RC18, dual-axis tracker.

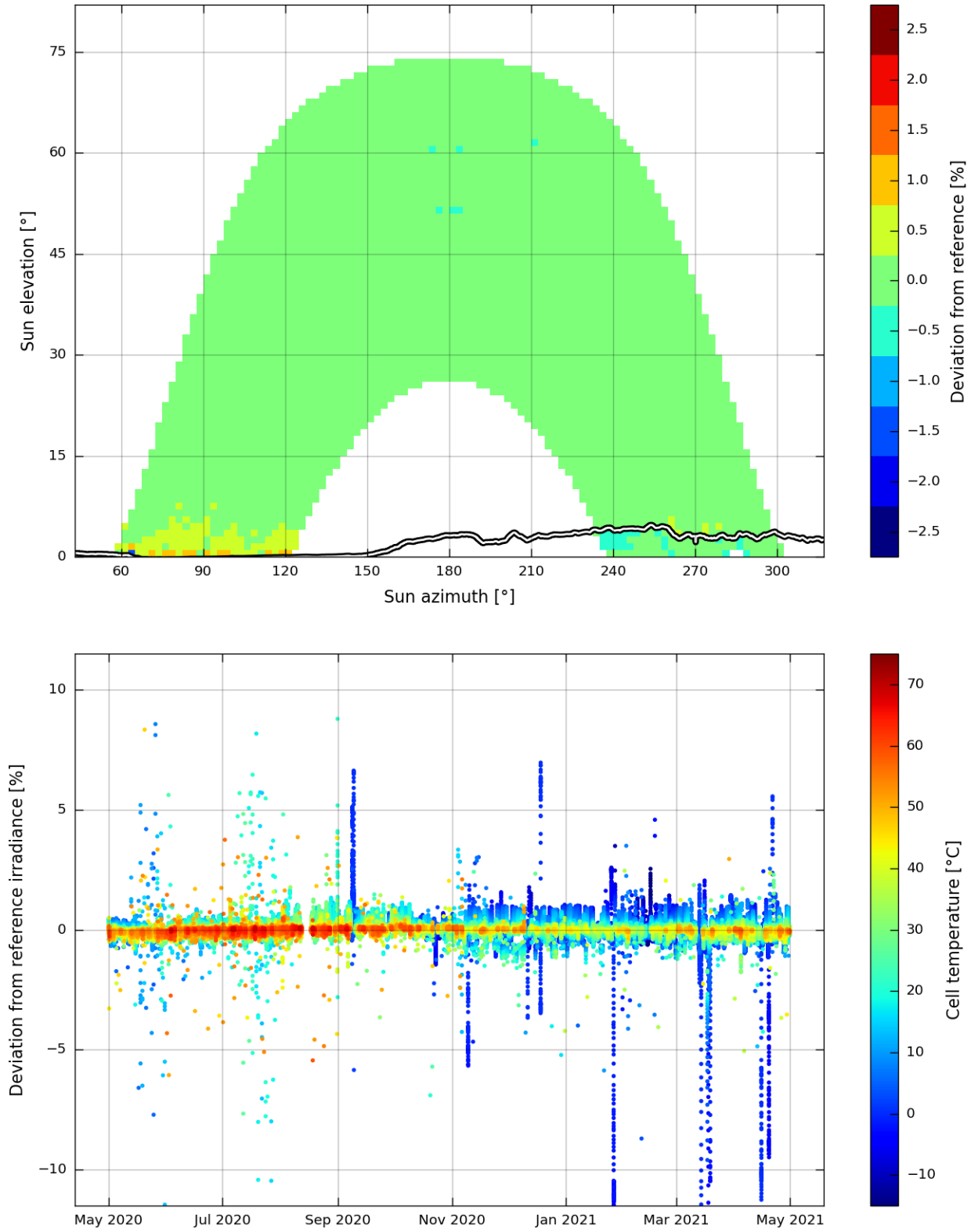

Figure A-12 Detailed results for model Si2, dual-axis tracker.

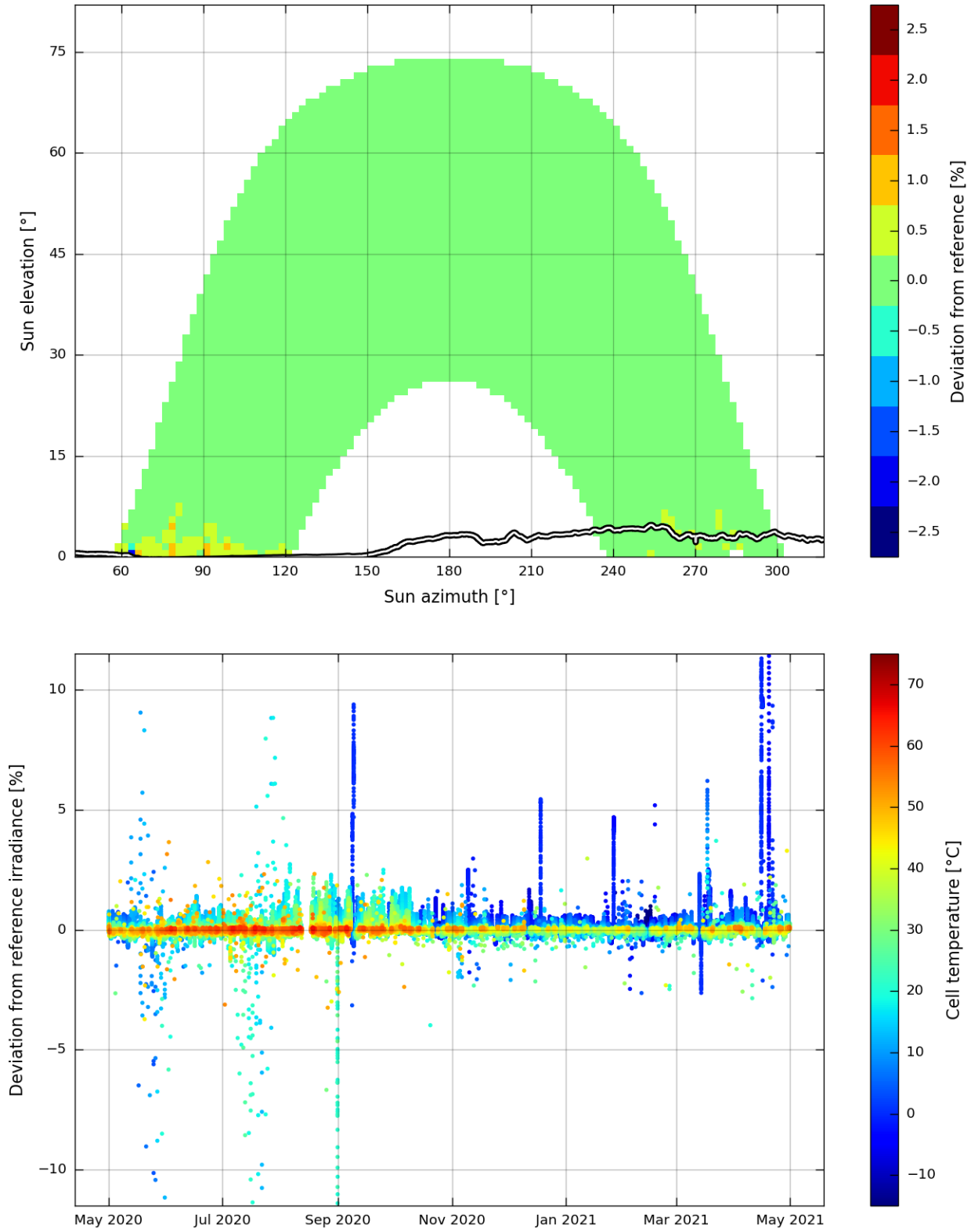

Figure A-13 Detailed results for model SOZ-03, dual-axis tracker.

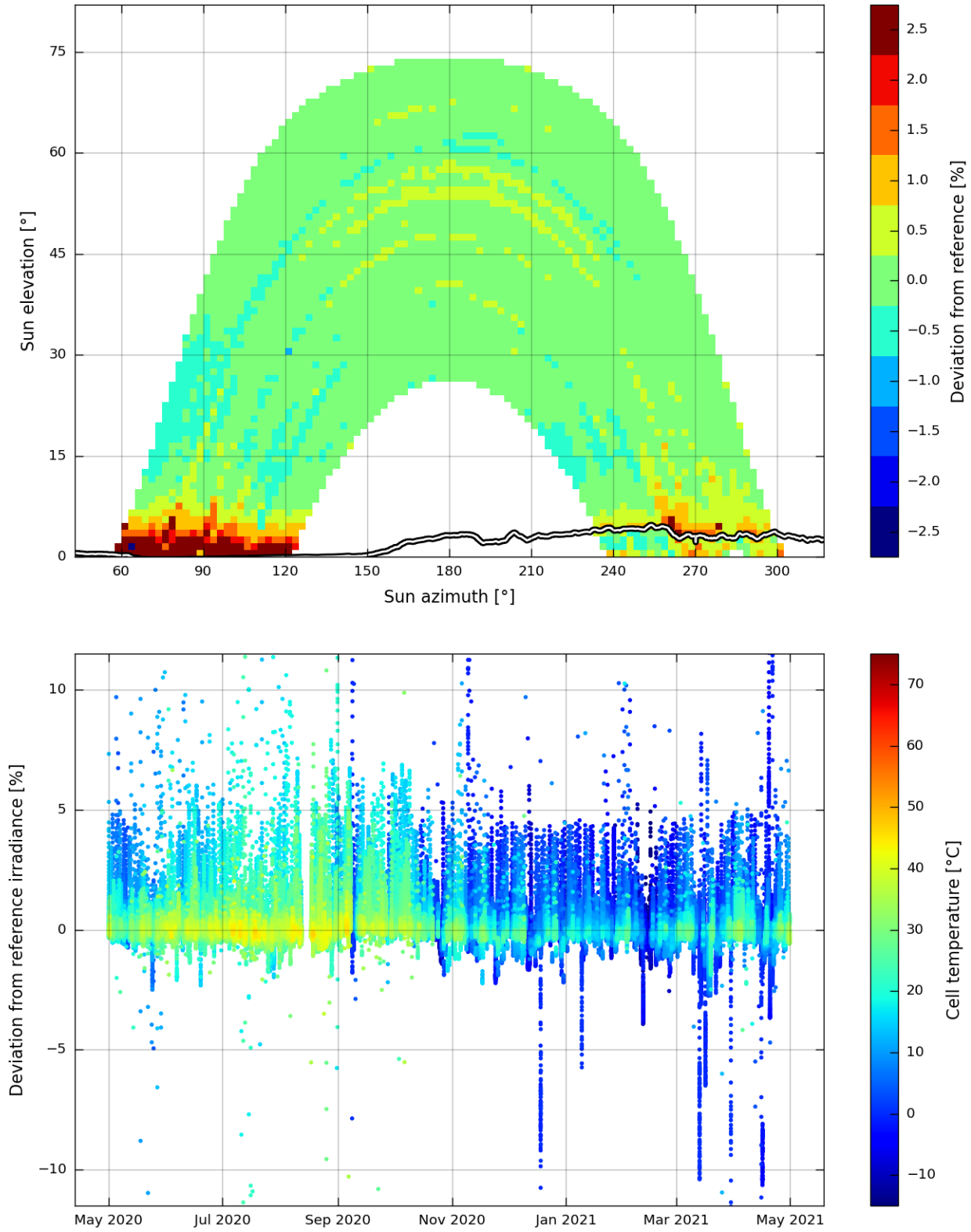

Figure A-14 Detailed results for model WPVS, dual-axis tracker.

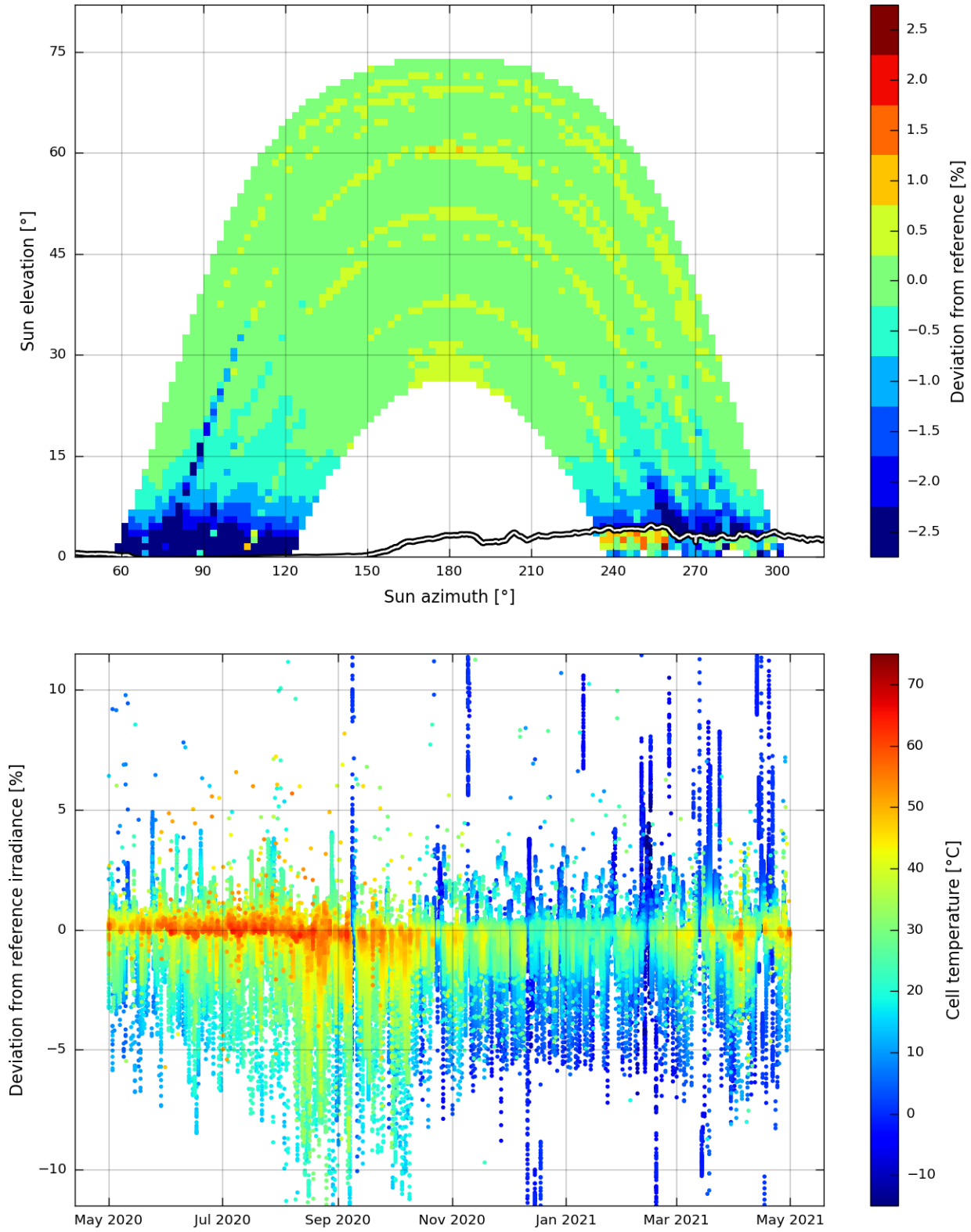

Figure A-15 Detailed results for model ISET, single-axis tracker.

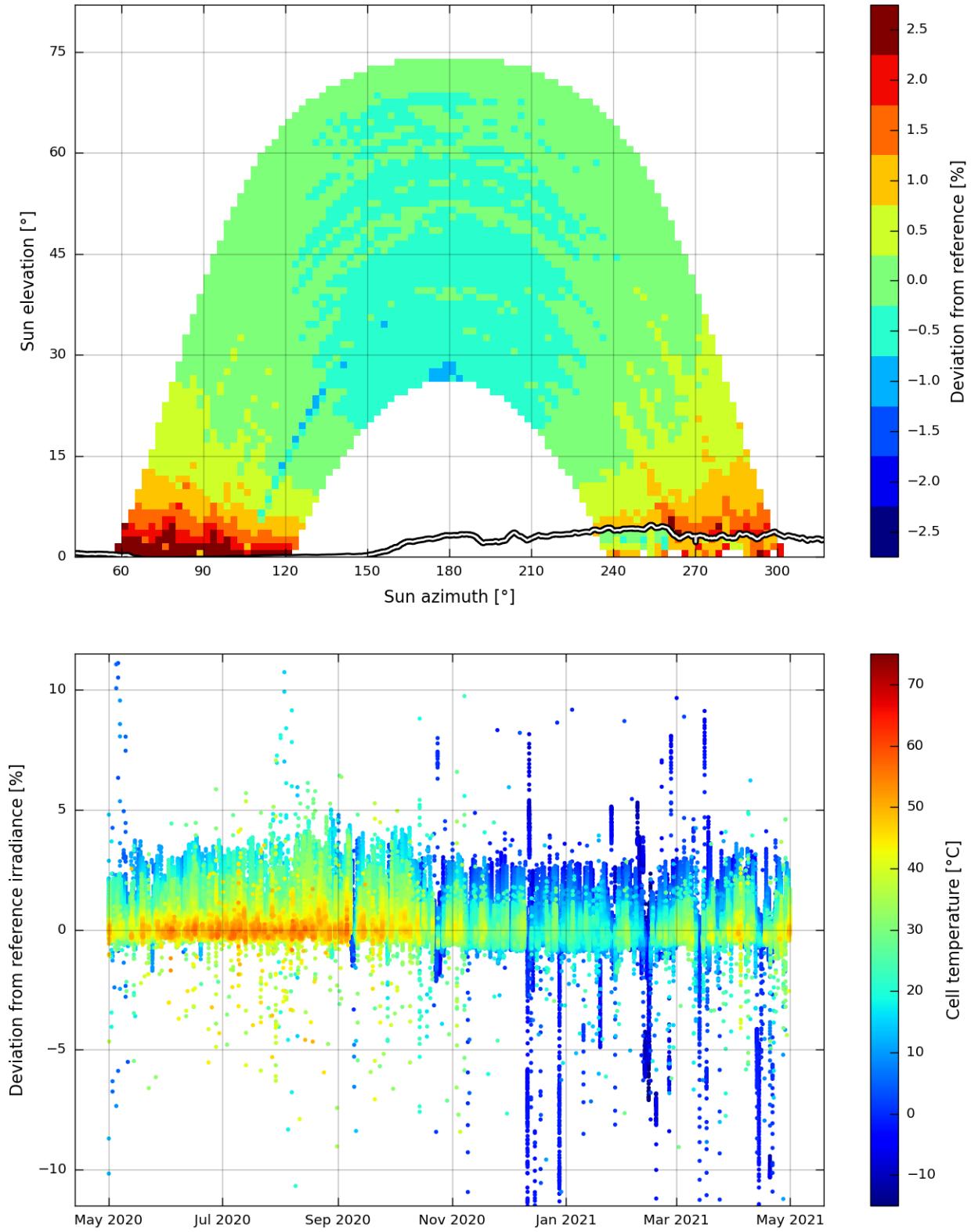

Figure A-16 Detailed results for model RC01, single-axis tracker.

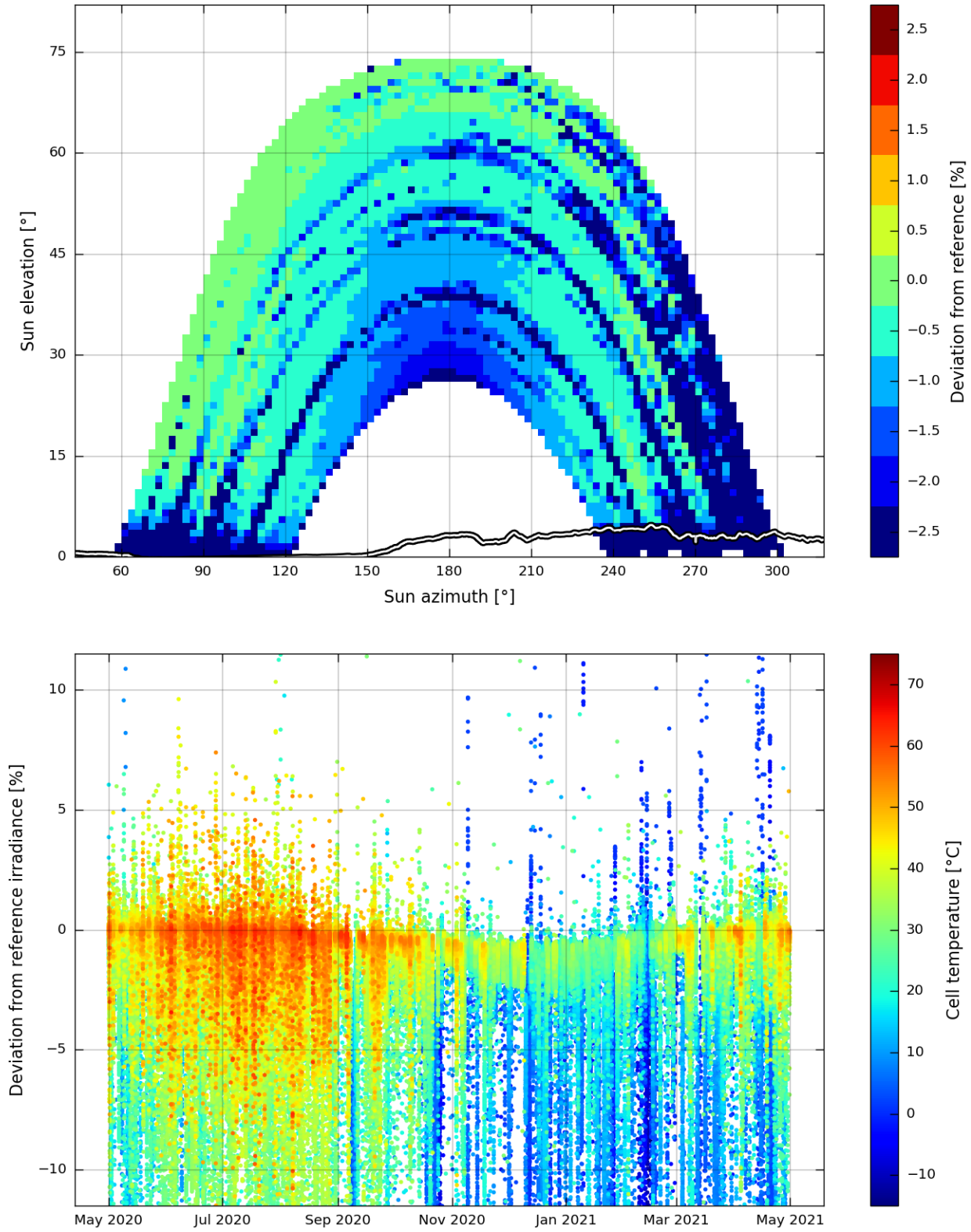

Figure A-17 Detailed results for model RC18, single-axis tracker.

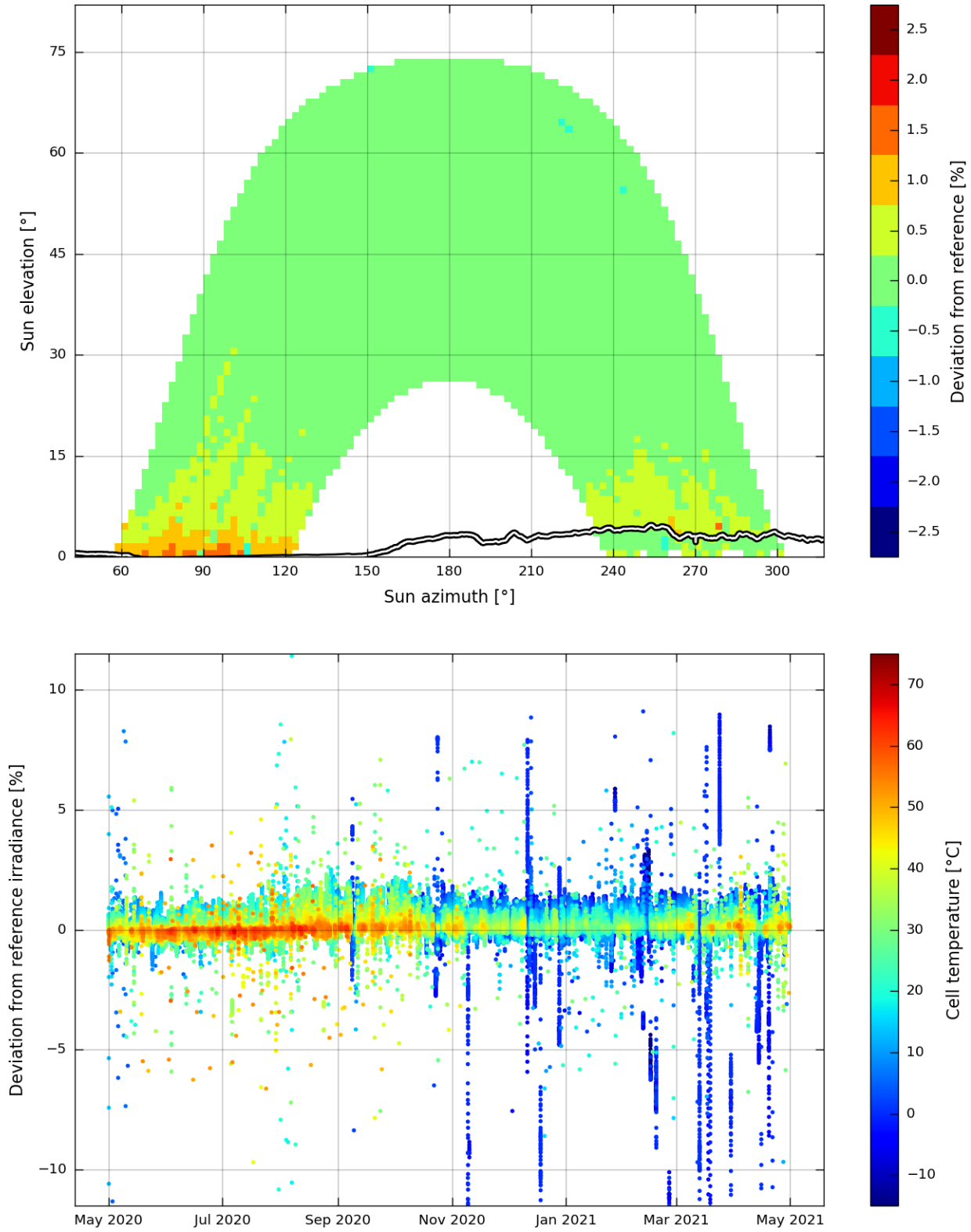

Figure A-18 Detailed results for model Si2, single-axis tracker.

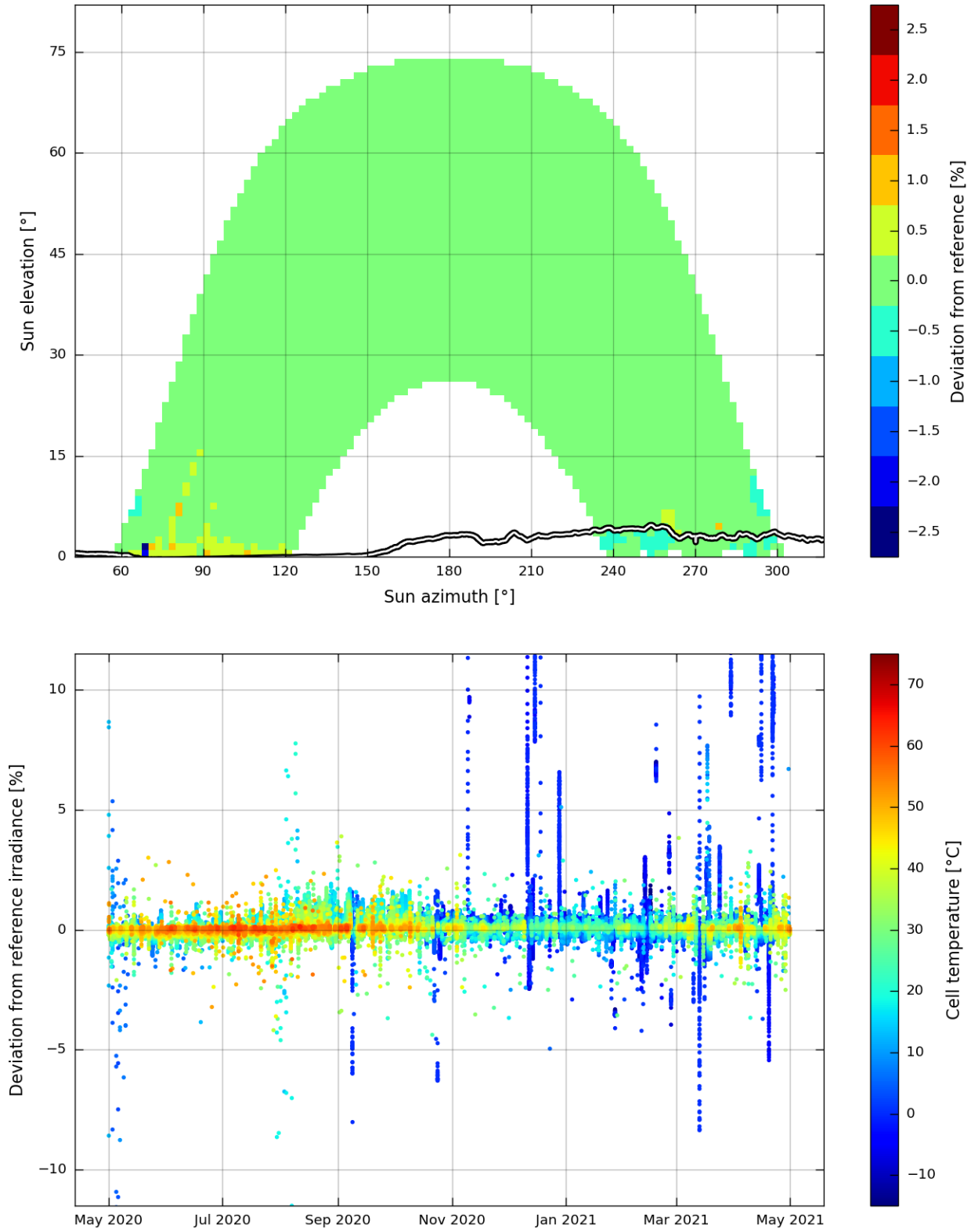

Figure A-19 Detailed results for model SOZ-03, single-axis tracker.